Wave propagation in slowly varying waveguides using a finite element approach

A. T. Fabro[a,*], N. S. Ferguson[b], B. R. Mace[c]

[a]Department of Mechanical Engineering, University of Brasilia, Brazil
[b]ISVR, University of Southampton, Southampton, UK
[c]Acoustics Research Centre, Department of Mechanical Engineering, University of Auckland, New Zealand

Abstract

This work investigates structural wave propagation in one dimensional waveguides with randomly varying properties along the axis of propagation, specifically when the properties vary slowly enough such that there is negligible backscattering, even if the net change is large. Wave-based methods are typically applied to homogeneous waveguides but the WKB (after Wentzel, Kramers and Brillouin) approximation can be used to find a suitable generalisation of the wave solution in terms of the change of phase and amplitude but is restricted to analytical solutions. A wave and finite element (WFE) approach is proposed to extend the applicability of the WKB method to cases where no analytical solution of the equations of motion is available. The wavenumber is expressed as a function of the position along the waveguide. A Gauss-Legendre quadrature scheme is subsequently used to obtain the phase change, while the wave amplitude is calculated using conservation of power. The WFE method is used to evaluate the wavenumbers at each integration point. Moreover, spatially correlated randomness can be included in the formulation by random field properties and in this paper is expressed by a Karhunen-Loève expansion. Numerical examples are compared to a standard FE approach and to available analytical solutions. They show good agreement when compared to either a full FE or analytical solution and require only a few WFE evaluations, providing a suitable framework for efficient stochastic analysis in waveguides.

Keywords: Wave propagation, Finite element, WKB approximation, Random field, Karhunen-Loève expansion

1. Introduction

Wave-based methods commonly assume that waveguide properties are homogeneous in the direction of wave propagation, limiting the application of such approaches. This assumption arises mainly because analytical solutions for non-homogeneous waveguides are only possible for very particular cases, for example acoustic horns, ducts, rods and beams, e.g. [1–4]. Moreover, randomly varying material and geometric properties along the axis of propagation play a significant role in the so-called mid-frequency region.

Wave solutions for non-homogeneous waveguides can be found by applying the classical WKB approximation [5–8]. Named after Wentzel, Kramers and Brillouin, it was initially developed for solving the Schrödinger equation in quantum mechanics. The formulation assumes that the waveguide properties vary slowly enough spatially such that there are no or negligible reflections due to these local changes, even if the net change is large. It maintains the wave-like interpretation of non-uniform

*Corresponding author
Email address: fabro@unb.br (A.T. Fabro)

waveguides, but it is restricted to available analytical solutions. Pierce [9] presented a physical interpretation for inhomogeneous beams and plates, deriving the leading terms of the approximation in terms of conservation of power. Recently, Nielsen and Sorokin [10] generalised the WKB method with applications to Rayleigh and Timoshenko beam theories in curved waveguides, using a FE model as a benchmark solution. Additionally, they have also shown that the energy flux conservation property leads to the exact amplitude function to the leading order of the approximation. Moreover, Foucaud et al. [11] have experimentally shown the validity of the WKB model for a plate of varying thickness immersed in a fluid connected to an acoustic black hole, modelling a passive cochlea. They have also shown experimentally the variation of the wavenumber as a function of position, a working assumption of the WKB method.

The fact that the wavenumber is a function of the position in a slowly varying waveguide can lead to the situation in which, for a given frequency, there could exist a part of the waveguide in which a particular wave mode is propagating in one region while it becomes non-propagating in another region. The transition between these two regions, a cut-on or cut-off transition, is known as a critical section or turning point [12] and leads to wave reflection due to the sudden change of the characteristics of wave propagation, even though the mechanical properties are slowly varying. In this region, the WKB approximation is no longer valid and a uniformly valid solution is required (e.g. [8,13,14]).

In engineering applications, manufacturing variability introduces variability in homogeneous or periodic structures affecting the dynamic performance of the designed structure [15]. Typically, this variability is such that it can be spatially varying with some degree of spatial correlation. Random field theory provides the means for a probabilistic representation of this variability and typically involves expressions for the probability density function together with a model for the spatial variability of the properties, given by a correlation function and correlation length, for a second order homogeneous random field [16]. The most commonly used methods of representing a random field in a mechanical model include the use of series expansions, such as the Karhunen-Loève (KL) decomposition or the Polynomial Chaos expansion [17]. Fabro et al. [18] have applied the WKB method to investigate wave propagation in rods and beams with spatially correlated randomness, using random field theory. An experimental validation was also presented showing the validity of the approximation for low order beam theory using a set of randomly distributed added masses [18] and for chopped fibre composite beams [19].

Waveguides with complicated cross-sections, such as laminates or sandwich-structured composites, typically have no analytical solution available, so the WKB formalism cannot be directly applied. For such cases involving homogeneous or periodic waveguides, the wave and finite element (WFE) approach can be applied. The WFE is a wave-based method that is used to predict the wavenumbers and wave modes of a waveguide from a finite element (FE) model of a small segment of the waveguide, by postprocessing the mass and stiffness matrices typically obtained from a commercial or in-house FE package. This method has been applied to a number of cases in structural dynamics including free and forced vibration [20–28]. Because of its computational efficiency, the WFE approach offers a suitable framework for the analysis of randomness in periodic structures, but its applications have been limited to spatially homogeneous randomness [29–31], even though it can be used to model non-uniform cross-sections.

In this work, a WFE approach is proposed to model waveguides with slowly varying properties using conservation of the time-averaged energy flow, which is in principle equivalent to the WKB approximation to its leading order, as described by Pierce [9]. Therefore, the wave properties are calculated using the WFE approach and they are expressed as a function of the position along the waveguide. The phase change of a propagating wave over a distance is calculated using a Gauss-

Legendre quadrature scheme for numerical integration of the local wavenumber. The WFE method is used to evaluate the wavenumbers at each integration point, and these are kept to a minimum to reduce computation cost while still being able to capture the non-homogeneity to a given specified level of accuracy. The wave amplitude change is calculated using conservation of power.

Various numerical examples comprising a rod, beam and plate strip with non-uniform material and geometrical properties are considered. Results obtained from deterministic and stochastic examples are compared to standard FE and analytical solutions, the latter when available. Spatially correlated randomness is given by a KL expansion. Results show good agreement and require only a few WFE evaluations, providing a suitable framework to account for spatially correlated randomness in waveguides.

In the next section, the WKB approximation is briefly reviewed and described in terms of propagation and reflection matrices for the forced response of a finite length waveguide. In section 3, the WFE approach is reviewed and, in Section 4, a framework for introducing slowly varying properties along the lines of the WKB assumption to a WFE formulation is proposed. Section 5 presents numerical results for waveguides with properties that vary along the waveguide. Rods, beams and plate strips with varying and known (i.e. deterministic) material and geometric properties are considered. Section 6 introduces random variability using the KL expansion for Gaussian and non-Gaussian random fields. Even though results in this work are given for an analytical expression of the KL expansion for an exponentially decaying correlation function, it is straightforward to extend them for other numerical solutions. Section 6 then presents numerical examples of rods, beams and plate strips with stochastic properties. Finally, concluding remarks are given in section 7.

2. The WKB approximation

The WKB formulation has been applied in many fields of engineering, including acoustics [12,32] and structural dynamics [9,10,18,33,34]. However, the WKB approximation breaks down if the properties change rapidly or when the travelling wave reaches a local cut-off section where the wave mode ceases to propagate. This transition, also known as a turning point or critical section, leads to an internal reflection, breaking down the main assumption in the theory and requiring a different approximation for certain frequency bands [7,35]. Uniformly valid approximations, i.e., solutions valid close and far from the critical section can be derived. A single turning point can happen in different positions for different frequencies [13,14]), or it is possible to have the presence of more than one turning point, creating the effect of wave tunnelling, if two turning points are close together [8].

Assuming a time harmonic solution, $u(x,t) = U(x)\,\mathrm{e}^{\mathrm{i}\omega t}$, it is possible to define a local wavenumber $k(x)$. Thus, the *eikonal* function $S(x) = \log \widetilde{U}(x) + \mathrm{i}\theta(x)$ is introduced, in order to find wave solutions of the kind [6]

$$U(x) = \mathrm{e}^{S(x)} = \widetilde{U}(x)\mathrm{e}^{\pm \mathrm{i}\theta(x)}. \tag{1}$$

Suppose there are n wave modes in the waveguide propagating in both the positive and negative directions. Given vectors of the amplitudes of the positive and negative going waves $\mathbf{a}^+$, $\mathbf{a}^-$, $\mathbf{b}^+$ and $\mathbf{b}^-$, it is possible to define positive and negative going propagation matrices for waves travelling between x_a and x_b [18], such that $\mathbf{b}^+ = \boldsymbol{\Lambda}^+(x_a, x_b)\mathbf{a}^+$ and $\mathbf{a}^- = \boldsymbol{\Lambda}^-(x_b, x_a)\mathbf{b}^-$, where

$$\begin{aligned} \boldsymbol{\Lambda}^+(x_a, x_b) &= \mathrm{diag}\left[\exp\left(-\mathrm{i}\theta_j(x_a, x_b) + \gamma_j(x_a, x_b)\right)\right], \\ \boldsymbol{\Lambda}^-(x_b, x_a) &= \mathrm{diag}\left[\exp\left(-\mathrm{i}\theta_j(x_a, x_b) - \gamma_j(x_a, x_b)\right)\right], \end{aligned} \tag{2}$$

where diag[·] stands for a diagonal matrix and, for the general case of a complex wavenumber [36]

$$\theta_j(x_a,x_b)=\int_{x_a}^{x_b}\mathrm{Re}\{k_j(x)\}dx+\mathrm{i}\int_{x_a}^{x_b}\mathrm{Im}\{k_j(x)\}dx \text{ and } \gamma_j(x_a,x_b)=\log\left(\left|\frac{b^+}{a^+}\right|\right). \tag{3}$$

The real part of $\theta_j(x_a,x_b)$ is related to the phase change while the imaginary part of $\theta_j(x_a,x_b)$ is related to the wave attenuation due to damping. For a propagating wave in an undamped medium θ is pure real. The term $\gamma_j(x_a,x_b)$ is the wave amplitude change due to changes in the waveguide properties. Note that the latter causes $\mathbf{\Lambda}^+(x_a,x_b)\neq\mathbf{\Lambda}^-(x_b,x_a)$, unlike the homogeneous case.
Additionally, the response to a point force can be considered as illustrated in Figure 1. The wave amplitudes at the excitation point are given by

$$\mathbf{c}^+=\mathbf{e}^+ +\mathbf{b}^+ \text{ and } \mathbf{b}^-=\mathbf{e}^- +\mathbf{c}^-, \tag{4}$$

where $\mathbf{e}^+$ and $\mathbf{e}^-$ are the amplitudes of the waves directly generated by the excitation and which can be calculated from equilibrium and continuity conditions. Wave amplitudes at the boundaries are related by the reflection matrices as $\mathbf{a}^+=\mathbf{\Gamma}_L\mathbf{a}^-$ and $\mathbf{d}^-=\mathbf{\Gamma}_R\mathbf{d}^+$. The travelling wave amplitudes are related by the propagation matrices as $\mathbf{b}^+=\mathbf{\Lambda}^+(0,L_e)\mathbf{a}^+$, $\mathbf{d}^+=\mathbf{\Lambda}^+(L_e,L)\mathbf{c}^+$, $\mathbf{a}^-=\mathbf{\Lambda}^-(L_e,0)\mathbf{b}^-$, $\mathbf{c}^-=\mathbf{\Lambda}^-(L,L_e)\mathbf{d}^-$, $\mathbf{h}^+=\mathbf{\Lambda}^+(L_e,L_r)\mathbf{c}^+$ and $\mathbf{h}^-=\mathbf{\Lambda}^-(L,L_r)\mathbf{d}^-$.

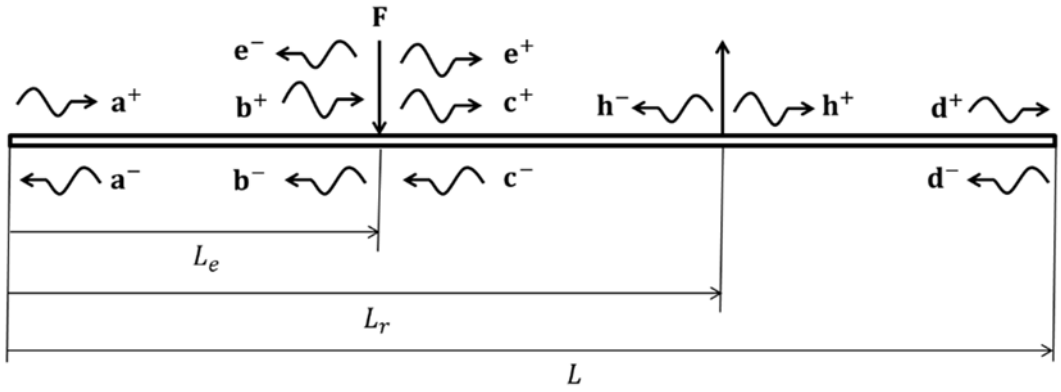

Figure 1. Point excitation and wave amplitudes on a waveguide with slowly varying properties.

These relations can be used to find

$$\mathbf{c}^+=[\mathbf{I}-\mathbf{\Lambda}^+(0,L_e)\mathbf{\Gamma}_L\mathbf{\Lambda}^-(L,0)\mathbf{\Gamma}_R\mathbf{\Lambda}^+(L_e,L)]^{-1}[\mathbf{e}^+ +\mathbf{\Lambda}^+(0,L_e)\mathbf{\Gamma}_L\mathbf{\Lambda}^-(L_e,0)\mathbf{e}^-], \tag{5}$$

$$\mathbf{c}^-=\mathbf{\Lambda}^-(L,L_e)\mathbf{\Gamma}_R\mathbf{\Lambda}^+(L_e,L)\mathbf{c}^+, \tag{6}$$

from which the forced response can be calculated. The same rationale can be used to calculate the response at any point in the waveguide from the wave amplitudes $\mathbf{h}^+$ and $\mathbf{h}^-$.

3. The wave and finite element approach

In this section, a brief review of the WFE approach is presented for one-dimensional periodic or homogeneous waveguide. A section of the waveguide of axial length Δ is cut from the structure and, assuming harmonic motion, its dynamic stiffness matrix $\widetilde{\mathbf{D}}=\mathbf{K}+\mathrm{i}\omega\mathbf{C}-\omega^2\mathbf{M}$ can be obtained from a conventional FE analysis, such that $\widetilde{\mathbf{D}}\mathbf{q}=\mathbf{f}$, where $\mathbf{K}$, $\mathbf{C}$ and $\mathbf{M}$ are, respectively, the stiffness, damping

and mass matrices, $\mathbf{q}$ is the vector of nodal degrees of freedom and $\mathbf{f}$ is the vector of nodal forces. The dynamic stiffness matrix $\widetilde{\mathbf{D}}$ can be condensed to eliminate any interior degrees of freedom, leading to the matrix $\mathbf{D}$ that can be partitioned as

$$\begin{bmatrix} \mathbf{D}_{LL} & \mathbf{D}_{LR} \\ \mathbf{D}_{RL} & \mathbf{D}_{RR} \end{bmatrix} \begin{bmatrix} \mathbf{q}_L \\ \mathbf{q}_R \end{bmatrix} = \begin{bmatrix} \mathbf{f}_L \\ \mathbf{f}_R \end{bmatrix}, \tag{7}$$

relating the degrees of freedom and nodal forces on the left (L) and the right (R) cross-sections [20]. For a wave freely propagating along the waveguide, a propagation constant relates displacements and forces at the left and right sides of the section s, i.e. $\mathbf{q}_R^s = \lambda \mathbf{q}_L^s$ and $\mathbf{f}_R^s = -\lambda \mathbf{f}_L^s$. Moreover, from continuity of displacements and equilibrium of forces between sections s and $(s+1)$ it follows that $\mathbf{q}_L^{s+1} = \mathbf{q}_R^s$ and $\mathbf{f}_L^{s+1} = -\mathbf{f}_R^s$. Then, a transfer matrix can be defined such that

$$\begin{bmatrix} \mathbf{q}_L^{s+1} \\ \mathbf{f}_L^{s+1} \end{bmatrix} = \mathbf{T} \begin{bmatrix} \mathbf{q}_L^{s} \\ \mathbf{f}_L^{s} \end{bmatrix}, \tag{8}$$

where

$$\mathbf{T} = \begin{bmatrix} -\mathbf{D}_{LR}^{-1}\mathbf{D}_{LL} & \mathbf{D}_{LR}^{-1} \\ -\mathbf{D}_{RL} + \mathbf{D}_{RR}\mathbf{D}_{LR}^{-1}\mathbf{D}_{LL} & -\mathbf{D}_{RR}\mathbf{D}_{LR}^{-1} \end{bmatrix}. \tag{9}$$

The eigenvalues and eigenvectors of the transfer matrix can be separated into two sets related to the n positive-going waves (λ_j and $\boldsymbol{\phi}_j^+$) and the n negative-going waves ($1/\lambda_j$ and $\boldsymbol{\phi}_j^-$). The eigenvectors correspond to wave modes and the j^{th} eigenvalue can be written as $\lambda_j = \exp(-\mathrm{i}k_j\Delta)$. The eigenvectors can be partitioned such that $\boldsymbol{\phi}^+ = \begin{bmatrix} \boldsymbol{\phi}_q^+ \\ \boldsymbol{\phi}_f^+ \end{bmatrix}$ and $\boldsymbol{\phi}^- = \begin{bmatrix} \boldsymbol{\phi}_q^- \\ \boldsymbol{\phi}_f^- \end{bmatrix}$. These are used to define a linear transformation

$$\mathbf{q}_L = \boldsymbol{\phi}_q^+ \mathbf{a}^+ + \boldsymbol{\phi}_q^- \mathbf{a}^- \text{ and } \mathbf{f}_L = \boldsymbol{\phi}_f^+ \mathbf{a}^+ + \boldsymbol{\phi}_f^- \mathbf{a}^-, \tag{10}$$

from the wave domain (in terms of wave amplitudes $\mathbf{a}^+$ and $\mathbf{a}^-$) to the physical domain (i.e. nodal DOFs and forces). Note that, due to the assumption that the waveguide is homogeneous, the wave modes are the same at any given position of the waveguide. This is unlike the non-homogeneous case. When damping is considered, then $|\lambda_j| < 1$ for positive-going waves [26]. Additionally, any boundary condition can be written algebraically as $\mathbf{A}\mathbf{f} + \mathbf{B}\mathbf{q} = \mathbf{0}$. Then the reflection matrices are given by [4,26]

$$\boldsymbol{\Gamma}_L = -\left(\mathbf{A}\boldsymbol{\phi}_{\mathrm{f}}^+ + \mathbf{B}\boldsymbol{\phi}_{\mathrm{q}}^+\right)^{-1}\left(\mathbf{A}\boldsymbol{\phi}_{\mathrm{f}}^- + \mathbf{B}\boldsymbol{\phi}_{\mathrm{q}}^-\right) \text{ and } \boldsymbol{\Gamma}_R = -\left(\mathbf{A}\boldsymbol{\phi}_{\mathrm{f}}^- + \mathbf{B}\boldsymbol{\phi}_{\mathrm{q}}^-\right)^{-1}\left(\mathbf{A}\boldsymbol{\phi}_{\mathrm{f}}^+ + \mathbf{B}\boldsymbol{\phi}_{\mathrm{q}}^+\right). \tag{11}$$

The amplitudes of the positive and negative going waves generated by a point excitation can be calculated using Eq. (10) along with continuity and equilibrium conditions, leading to [25,26]

$$\begin{bmatrix} \boldsymbol{\phi}_{\mathrm{q}}^+ & -\boldsymbol{\phi}_{\mathrm{q}}^- \\ \boldsymbol{\phi}_{\mathrm{f}}^+ & -\boldsymbol{\phi}_{\mathrm{f}}^- \end{bmatrix} \begin{Bmatrix} \mathbf{e}^+ \\ \mathbf{e}^- \end{Bmatrix} = \begin{Bmatrix} \mathbf{0} \\ \mathbf{f}_{ext} \end{Bmatrix}, \tag{12}$$

which can be solved either by direct inversion or by using the orthogonality properties of the left eigenvector of the transfer matrix, which improves numerical conditioning [24,25]. The response to general spatially distributed excitation can be calculated following the procedure given by Renno and

Mace [26]. A number of parameters yielding information about the wave propagation characteristics can be calculated from this approach. In this work, it is particularly interesting to calculate the time average power transmitted through the cross-section, i.e.

$$P = -\frac{1}{2}\mathrm{Re}\{\mathrm{i}\omega \mathbf{f}_{\mathrm{L}}^{H}\mathbf{q}_{\mathbf{L}}\} = \frac{\omega}{2}\mathrm{Im}\{\mathbf{f}_{\mathrm{L}}^{H}\mathbf{q}_{\mathrm{L}}\}, \tag{13}$$

where the superscript H stands for the Hermitian. For the undamped case, if $|\lambda_j| = 1$, the wave is positive-going when $P > 0$.

4. Wave and finite element approach with slowly varying properties

Under the assumptions of the WKB approximation, it is necessary to calculate the phase change considering the locally defined wavenumber $k_j(x)$ as well as the amplitude change caused by the slowly varying waveguide properties. In this section, the WFE approach is used to estimate $k_j(x)$ at a number of points to calculate the phase change $\theta_j(x_a, x_b)$ from position x_a to x_b. A numerical integration using a Gauss-Legendre (GL) quadrature scheme is applied, i.e. [36]

$$\theta_j(x_a, x_b) = \int_{x_a}^{x_b} \mathrm{Re}\{k_j(x)\}dx + \mathrm{i}\int_{x_a}^{x_b} \mathrm{Im}\{k_j(x)\}dx \approx \sum_{i=1}^{N_{gl}} G_i\left[\mathrm{Re}\{k_j(x_i)\} + i\mathrm{Im}\{k_j(x_i)\}\right], \tag{14}$$

where G_i are the weights and $k_j(x_i)$ is the j^{th} wavenumber calculated at the sampling point x_i, defined from the GL quadrature. The properties are evaluated at x_i from a given function describing the spatial variability of these properties and then assumed constant within the segment used for the WFE. This is equivalent to a mid-point discretization for the spatial variability given by a random field within each segment. Therefore it is recommended, as a rule of thumb, that the segment size Δ is at least four times smaller than the random field correlation length [37–39]. The integration scheme gives the exact integral for a polynomial of a given order depending on the number of points N_{gl}, therefore it is the same as a polynomial fitting of the wavenumber over the waveguide between x_a and x_b. The number of points used by the quadrature should be kept to a minimum number of evaluations, to avoid excessive computational cost. Additionally, no re-meshing of the FE model is necessary for each WFE evaluation. Figure 2 shows the positions of the WFE evaluations for $N_{gl} = 3$ compared to the homogeneous case, in which only one WFE evaluation is necessary.

The forced response requires a number N_{gl} of WFE evaluations for the calculation of propagation matrices to the left and also to the right side of the excitation point, one evaluation at the left and right boundaries and one evaluation at the excitation point itself, with a total of $N_{eval} = 2N_{gl} + 3$ WFE evaluations, as represented in Figure 2. Note that an integration scheme which includes the points at the boundaries and at the point force could be used, such as Gauss-Lobato quadrature, for instance. That would further increase the computational efficiency of the proposed approach.

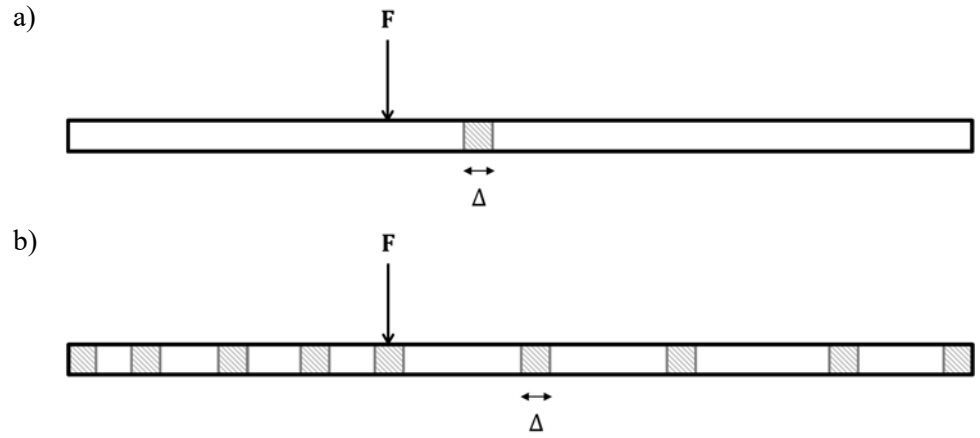

Figure 2. Segments for WFE evaluations for (a) homogeneous and (b) slowly varying waveguide at the Gauss-Legendre integration points x_i, for $N_{gl} = 3$.

The amplitude change can be calculated from energy conservation for an undamped system as a consequence of the WKB approximation [9]. It can be shown that the two approaches are equivalent to the leading order of the WKB approximation [10,34]. Therefore, for a positive-going wave travelling from x_a, with amplitude a^+, to x_b, with amplitude b^+, as shown in Figure 3, assuming no damping, the time average power (Eq. (13)) transmitted through the cross-sections, at the two positions must be equal, leading to

$$\left|a_j^+\right|^2 \mathrm{Re}\left\{i\omega \boldsymbol{\phi}_{f,j}^{+H}(x_a)\boldsymbol{\phi}_{q,j}^{+}(x_a)\right\} = \left|b_j^+\right|^2 \mathrm{Re}\left\{\mathrm{i}\omega \boldsymbol{\phi}_{f,j}^{+H}(x_b)\boldsymbol{\phi}_{q,j}^{+}(x_b)\right\}. \tag{15}$$

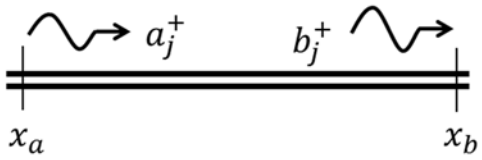

Figure 3. Positive-going wave travelling from x_a, with amplitude a_j^+, to x_b, with amplitude b_j^+, in an infinite waveguide.

Equation (15) can be rearranged in order to express the amplitude change, giving

$$\gamma_j(x_a, x_b) = \frac{1}{2}\log\left(\frac{\mathrm{Re}\left\{\mathrm{i}\omega \boldsymbol{\phi}_{f,j}^{+H}(x_a)\boldsymbol{\phi}_{q,j}^{+}(x_a)\right\}}{\mathrm{Re}\left\{\mathrm{i}\omega \boldsymbol{\phi}_{f,j}^{+H}(x_b)\boldsymbol{\phi}_{q,j}^{+}(x_b)\right\}}\right). \tag{16}$$

Both $\theta_j(x_a, x_b)$ and $\gamma_j(x_a, x_b)$ are then used to calculate the positive and negative going propagation matrices, defined by Eq. (2). Note that, although the wave modes propagate independently, the wave mode shapes $\boldsymbol{\phi}_j^{\pm}(x)$ vary slowly along the slowly varying waveguide. Their amplitude change $\gamma_j(x_0, x)$, with respect to a reference position x_0, must be taken into account when calculating the response at an arbitrary position x of the waveguide. In principle, an interpolation scheme could be employed to that end using the evaluations at the GL points, further decreasing the computation cost.
Light damping can be included straightforwardly by calculating the complex wavenumber $k_j(x)$ at each segment using the WFE approach and then Eq. (14) is applied to calculate the total phase change and attenuation.

5. Numerical simulations for one-dimensional waveguides

In this section, some numerical examples are given for rods, beams and plate strips, with given variability in material and geometrical properties. The input mobility, i.e. velocity per unit force at the excitation position, is calculated for the rod and beam examples. In the rod example, the case of spatially varying Young's modulus is considered and the results obtained from the proposed approach and a standard model FE are presented. For the beam, two variable properties are considered. First, linearly varying thickness is considered in which results are compared with an available analytical solution. The second beam example assumes spatially varying Young's modulus and the results from the proposed approach are compared to a WKB approximation and a standard FE model. Finally, the case of a plate strip with simply supported edges and with linearly varying thickness is presented and the results are compared to the WKB approximation. In addition, a second example with spatially varying Young's modulus is presented in which the results are compared to a WKB approximation and a standard FE model. Simulations for random waveguides are presented in section 6.

5.1. Thin rod

For the case of longitudinal vibration in a straight thin rod, only a plane propagating wave is considered. The governing equation of motion with spatially varying Young's modulus $E(x)$ is given by

$$\rho A \frac{\partial^2 u(x,t)}{\partial t^2} - \frac{\partial}{\partial x}\left[E(x)A\frac{\partial u(x,t)}{\partial x}\right] = p(x,t), \tag{17}$$

where A is the area of the cross section, ρA is the mass per unit length, $p(x,t)$ is the excitation and $u(x,t)$ is the axial displacement. From the analytical WKB approximation, it is possible to define a local wavenumber $k_L(x) = \omega/c_L(x)$, where $c_L(x) = \sqrt{EA(x)/\rho A(x)}$ is the local phase velocity at position x. Assuming a time harmonic solution as in Eq. (1), thus $\widetilde{U}(x) = k_L^{-1/2}(x)$ and the amplitude change is given by $\gamma_L(x_a, x_b) = \frac{1}{2}\log[k_L(x_a)/k_L(x_b)]$ [18]. For a homogeneous undamped waveguide, $k_L = k_L(x)$ is a constant and the total phase change reduces to $\theta_L(0,L) = k_L L$, as well as there being no change in the amplitude, i.e. $\gamma_L(0,L) = 0$.

For the sample example, a FE model of a rod cross-section is built using a single element with two nodes and one degree of freedom per node, assuming constant properties within the element. The WFE approach is used to calculate the phase change by evaluating the wavenumber at the positions defined by the GL quadrature, Eq. (14), and the amplitude change is calculated from Eq. (16). More details are given in Appendix A.1.

5.1.1. Numerical results

In this section, a numerical example of longitudinal vibration is presented for an aluminium rod with spatially varying Young's modulus described by $E(x) = E_0[1 + H(x)]$, in which $E_0 = 70$GPa and $H(x)$ is a function describing the spatial variability, mass density $\rho = 2700$ kg/m^3, $L = 5$ m total length, rectangular cross-section 5 cm × 0.1 cm, free-free boundary conditions and point excitation at $L_e = 0.25L$. Structural damping is included using a complex Young's modulus $E(1 + \mathrm{i}\eta)$, with $\eta = 10^{-3}$. The function $H(x)$ was generated from a single sample of a Karhunen-Loève expansion

assuming $\sigma = 0.1$, correlation length $l_c = 0.5L$ and $N_{kl} = 10$ (see Section 6), and is shown in Figure 4 along with the excitation point and the points used for integration using GL quadrature.

Figure 5 shows the rod input mobility calculated using the slowly varying WFE approach using $N_{gl} = 8$ and $\Delta = 0.01$, i.e. fifty times smaller than l_c and within the required accuracy for the given frequency range. Results are compared to a full FE model with 300 elements, i.e. 150 times smaller than l_c. A mid-point random field discretization method is used in conjunction with the KL expansion [39] such that the Young's modulus $E(x)$ is sampled at the centre of each element with constant properties within the element [38]. A relative error measure is chosen such that

$$\Delta_{\text{avg}} = \frac{|\langle|\text{Y}|\rangle_B - \langle|\text{Y}_{\text{REF}}|\rangle_B|}{|\langle|\text{Y}_{\text{REF}}|\rangle_B|}, \tag{18}$$

in which $\langle\cdot\rangle_B$ is a frequency average over a frequency band B and $|\cdot|$ is the magnitude of the frequency response function. In this case, Y is the input mobility from the slowly varying WFE approach and Y_{REF} the reference FEM case. Errors in frequency averages are presented because of the presence of large errors at discrete frequencies around the resonance and antiresonance frequencies, which are a consequence of even small errors in the estimates of these frequencies. In addition, the frequency responses are calculated at discrete frequencies and a fine frequency resolution is needed to ensure that the errors due to discrete frequency sampling are small enough. In this paper the frequency resolution used to calculate frequency averages $\langle\cdot\rangle_B$ are smaller than 0.1 times the half-power bandwidth of a resonance at the centre of the frequency range under consideration. In the case of Figure 6, the resolution is 0.3 Hz.

Figure 6 presents the relative error of the frequency averaged response magnitudes obtained by the proposed approach and the standard FE solution for $N_{gl} = 8$ and $N_{gl} = 12$ points, using 15 equally spaced non-overlapping frequency bands of width B = 375 Hz and a frequency resolution of 0.3 Hz. A reduction in the error to less than 0.7% at high frequencies and less than 1 % at lower frequencies is found when increasing the number of GL points from $N_{gl} = 8$ to $N_{gl} = 12$ with $\eta = 10^{-3}$. Slightly higher error levels are found for $\eta = 10^{-2}$.

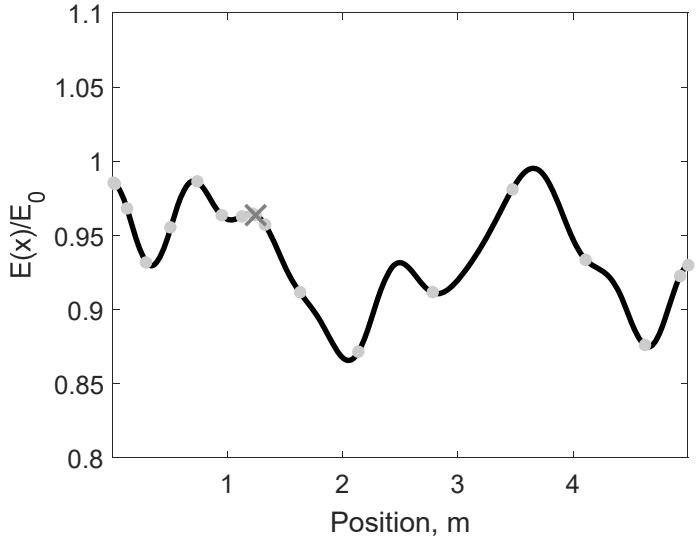

Figure 4. The normalized Young's modulus as a function of the position for the deterministic rod case. In addition, the WFE evaluation points (dot symbol) and excitation point (cross symbol) are shown.

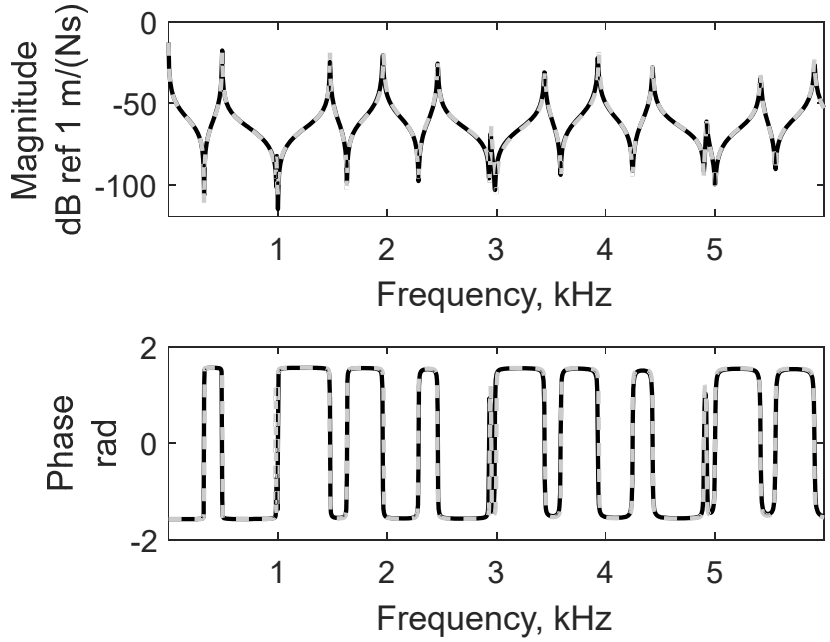

Figure 5. Magnitude and phase of the input mobility of the rod at $x = 0.25L$ using FE (black line) and the slowly varying WFE approach (grey dashed line) are shown.

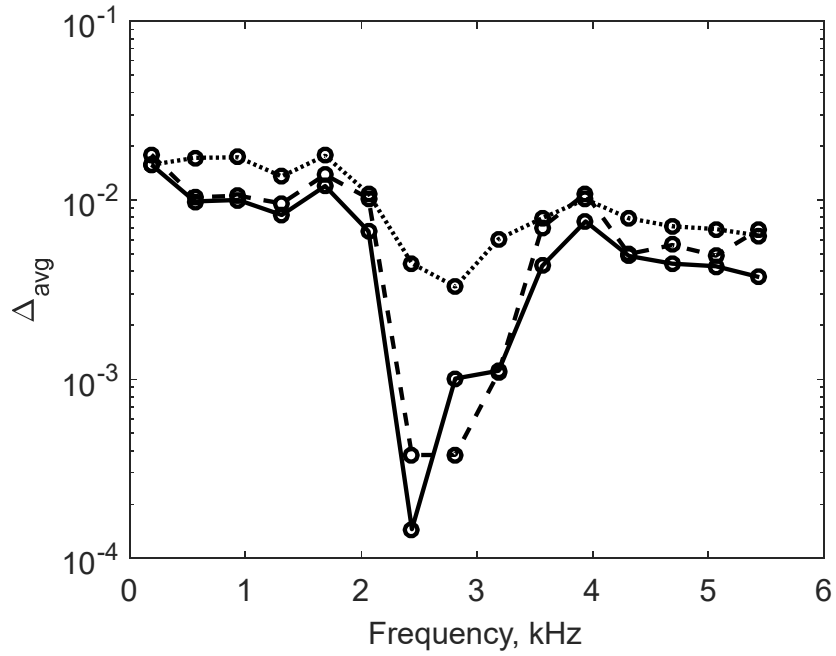

Figure 6. Relative error of the frequency averaged magnitude of the rod input mobility, compared to a full FE model, at $x = 0.25L$ with varying Young's modulus for different numbers of GL points: $N_{gl} = 8$ (dashed line), $N_{gl} = 12$ (full line) with $\eta = 10^{-3}$ and $N_{gl} = 12$ with $\eta = 10^{-2}$ (dotted line).

5.2. Thin beam

In this example, a Euler-Bernoulli beam undergoing flexural vibration with propagating and evanescent waves is considered. The proposed approach for wave propagation is applied for slowly varying material and geometrical properties.

In the case of flexural vibration of a beam, the governing equation of motion with spatially varying properties is given by

$$\frac{\partial^2}{\partial x^2}\left[EI(x)\frac{\partial^2 w(x,t)}{\partial x^2}\right] + \rho A(x)\frac{\partial^2 w(x,t)}{\partial t^2} = q(x,t), \tag{19}$$

where $EI(x)$ is the spatially varying bending stiffness, $q(x,t)$ is the excitation per unit length and $w(x,t)$ is the flexural displacement. Assuming a time harmonic solution $w(x,t) = W(x)\mathrm{e}^{-\mathrm{i}\omega t}$, the *eikonal* $S(x)$ is used here in order to find wave solutions of the kind $W(x) = \widetilde{W}(x)\mathrm{e}^{\pm\mathrm{i}\theta_B(x)}$, where $\widetilde{W}(x) = [\rho A(x)]^{-3/8}\,[EI(x)]^{-1/8}$ [9]. Propagating and evanescent waves are therefore taken into account, and then the propagation matrices are given by [18]

$$\boldsymbol{\Lambda}^{+}(x_a,x_b) = \mathrm{diag}\{\exp[-\mathrm{i}\theta_B(x_a,x_b) + \gamma_B(x_a,x_b)]\,, \exp[-\theta_B(x_a,x_b) + \gamma_B(x_a,x_b)]\}, \tag{20}$$

$$\boldsymbol{\Lambda}^{-}(x_a,x_b) = \mathrm{diag}\{\exp[-\mathrm{i}\theta_B(x_a,x_b) - \gamma_B(x_a,x_b)]\,, \exp[-\theta_B(x_a,x_b) - \gamma_B(x_a,x_b)]\}, \tag{21}$$

where the phase and amplitude changes are respectively given by Eq. (3).
A WFE model for a short segment of the beam is built using a single Euler-Bernoulli element with two nodes and two degrees of freedom per node [40] assuming constant properties within the element. Moreover, assuming that the material properties of the beam are constant while the cross-sectional area and the second moment of area are given by $A(x) = \alpha_A x^{\mu}$ and $I(x) = \alpha_I x^{\mu+2}$, where $\alpha_A > 0$, $\alpha_I > 0$, $x > 0$ and $\mu \geq 0$ is the flaring index, then an analytical solution of Eq. (19) can be found in terms of a linear combination of Hankel and modified Bessel functions representing positive and negative going propagating and evanescent waves [4], as presented in Appendix A.2.
Two cases of numerical examples are presented in the following sections. The first considers a non-uniform cross-sectional area while the second considers spatial variability of the Young's modulus. Specifically, the Young's modulus is modelled in the same way as in the previous example.
Both examples use an aluminium beam undergoing flexural vibration with constant mass density, with $L = 1$ m total length, free-free boundary conditions and point excitation at $L_e = 0.25L$. Structural damping is included using a complex Young's modulus $E(1 + \mathrm{i}\eta)$, with $\eta = 10^{-3}$. The wavenumbers from the WFE analysis were calculated with a segment length $\Delta = 0.01$ m.

5.2.1. Variable cross-section

In this case, the section is assumed to be rectangular with constant width $b = 10$ mm and linearly changing thickness, i.e. $\mu = 1$, with $h_L = 1$ mm at the left boundary and $h_R = 3$ mm at the right boundary and Young's modulus $E = 70$ GPa. Figure 7 shows the wavenumber divided by $\omega^{1/2}$ along the beam obtained from the analytical solution and with the WFE evaluations. Note that the position axis is defined from $x = 2$ m to $x = 3$ m, i.e. $L = 1$ m, due to the analytical formulation [4]. More details are given in Appendix A.2. Note that the results are in very good agreement and, for an increase in the thickness, the wavenumber decreases, because $k_B(x) \propto h^{-1/2}(x)$. Figure 8 shows the input mobility at $x = 0.25L$, using the analytical solution and the slowly varying WFE method. Here $N_{gl} = 3$ with the location of the points defined by the GL quadrature scheme and properties assumed to be constant within each segment. For calculation of the forced response a total of $N_{eval} = 2N_{gl} + 3 = 9$ WFE evaluations were needed.

Figure 9 presents the frequency averaged relative error of the proposed approach with respect to the analytical solution, using Eq. (18) and 10 equally spaced non-overlapping frequency bands of width $B = 45$ Hz, with frequency increments of 0.01 Hz, smaller than 0.1 times the half-power bandwidth at 250Hz, the centre of the frequency range considered. The overall error is smaller than 1.5%. No significant difference is found when increasing the number of GL integration points.

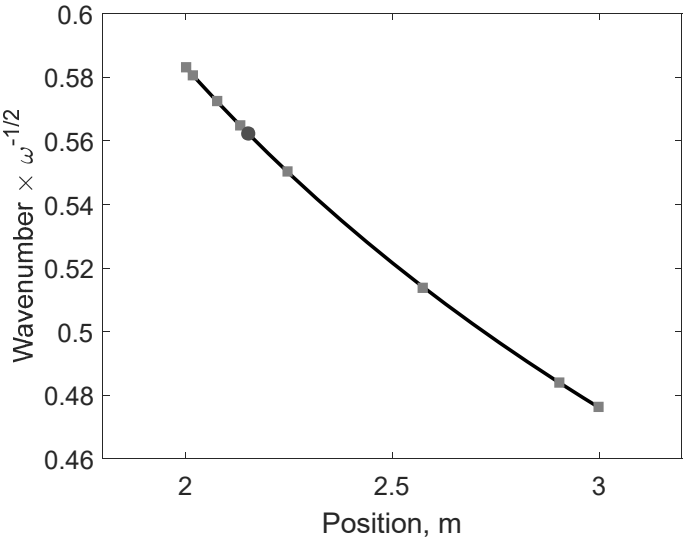

Figure 7. Normalized wavenumber with respect to $\omega^{1/2}$ along the beam with non-uniform linearly varying area using the analytical solution (black line), the WFE (grey square) and the excitation point location (grey circle), with $\mu = 1$.

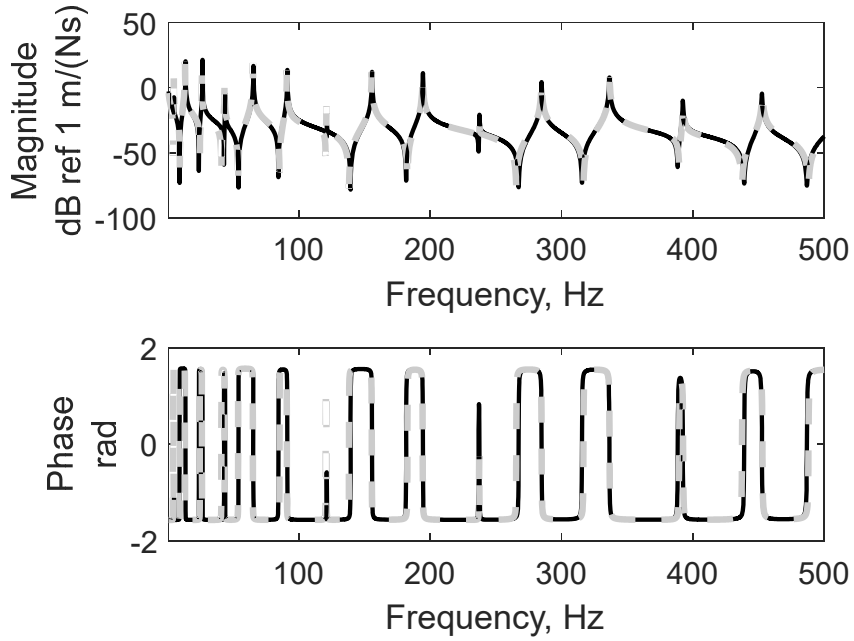

Figure 8. Magnitude and phase of the input mobility of the beam with linearly varying area at $x = 0.25L$ using the analytical solution (black solid) and the slowly varying WFE method (grey dashed).

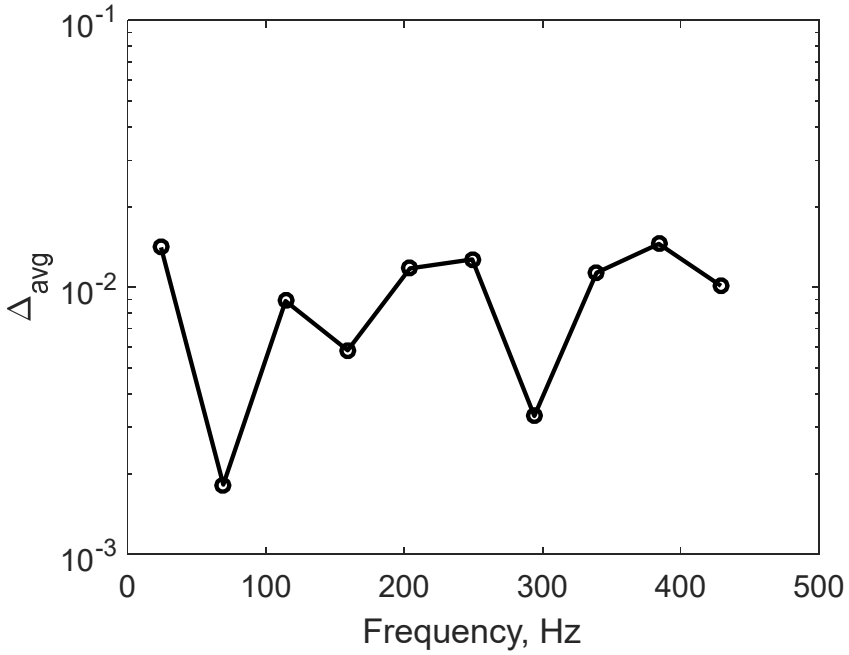

Figure 9. Beam with varying cross-sectional area: relative error of the frequency averaged magnitude of the beam input mobility at $x = 0.25L$, compared to the analytical solution.

5.2.2. Variable Young's modulus

In the second case, the Young's modulus is considered to vary in the same way as in the rod example (Figure 10) while the mass density and the geometric properties remain constant, with thickness $h = 1$ mm. Numerical results are compared to a standard FE model, with 300 elements and mid-point random field discretization (see Section 6), and to the analytical WKB approximation. Figure 11 shows the input mobility at $x = 0.25L$ using the standard FE model, the analytical WKB solution and the slowly varying WFE approach with $N_{gl} = 8$ points. Additionally, Figure 12 presents the frequency averaged relative error of the proposed approach with respect to the full FE method for $N_{gl} = 8$ (dashed line) and $N_{gl} = 12$ (dotted line), using 15 equally spaced non-overlapping frequency bands of width $B = 25$ Hz and a frequency increment of 0.01 Hz, equivalent to less than 0.1 times the half-power bandwidth at the centre of the frequency range under consideration. Overall, a slight improvement is found when increasing $N_{gl} = 8$ to $N_{gl} = 12$, with errors below 0.4% to 0.3 % at the low frequencies and from 0.3% to 0.1% at higher frequencies. For increasing damping to $\eta = 10^{-2}$, the error levels are slightly increased but still are overall smaller than 0.4%. It is not shown in Figure 12, but using the analytical WKB solution as the reference solution rather than the FE model produces extremely small relative errors around 10^{-6}%.

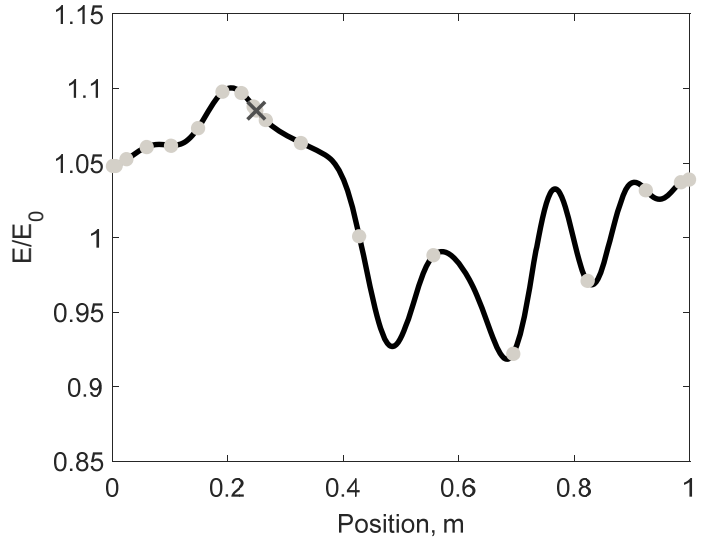

Figure 10. The normalized Young's modulus as a function of the position used for the deterministic beam case. In addition, the WFE evaluation points (dot symbols) and excitation point (cross symbol) are shown.

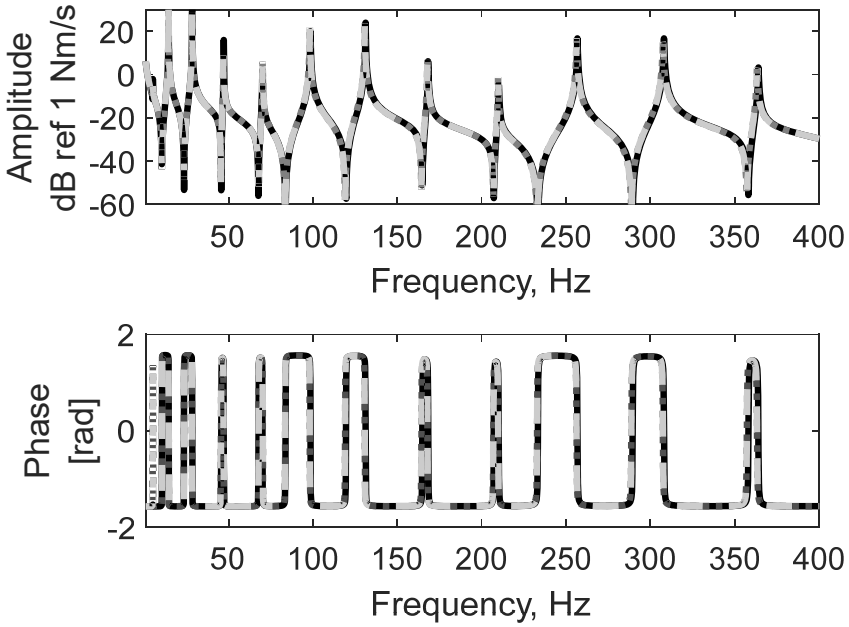

Figure 11. Beam with varying Young's modulus: magnitude and phase of the input mobility at $x = 0.25L$ using FE (black solid), analytical WKB (dark grey dotted) and the slowly varying WFE (light grey dashed).

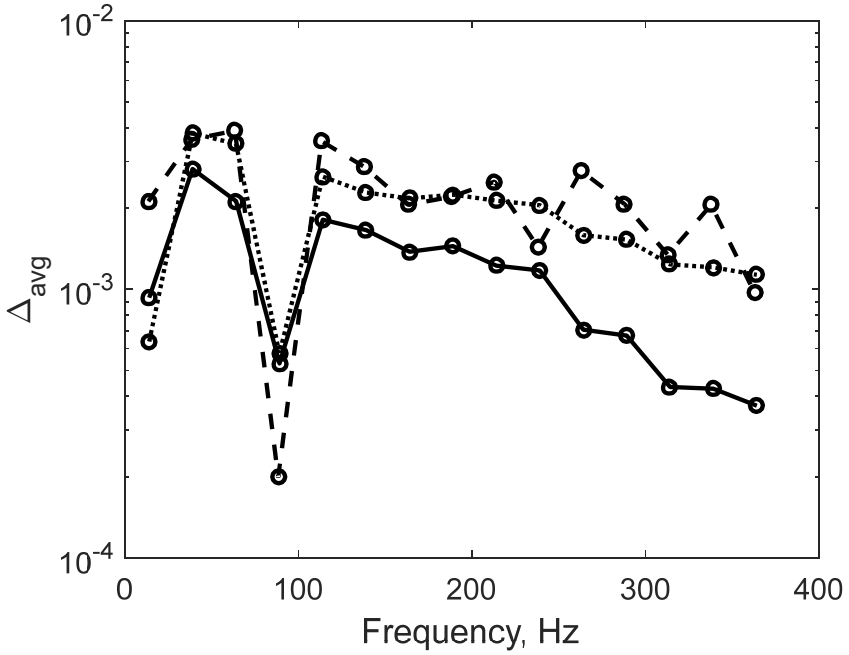

Figure 12. Beam with varying Young's modulus: relative error of the frequency averaged magnitude of the beam input mobility at $x = 0.25L$, compared to the full FE model, for $N_{gl} = 8$ (dashed line) and $N_{gl} = 12$ (solid line) with $\eta = 10^{-3}$ and $N_{gl} = 12$ with $\eta = 10^{-2}$ (dotted line).

5.3. Plate strip with simple supported edges

In this example, a rectangular plate strip with simply supported length-wise edges, and free ends, undergoing flexural vibration is considered, as shown in Figure 13. Setting a small parameter ϵ such that $\epsilon^{-4} = \omega^2$ and assuming solutions of the kind $w(x,y) = A(x,y)\mathrm{e}^{-\mathrm{i}\frac{\psi(x,y)}{\epsilon}}$, it is possible to derive an analytical governing equation, Appendix A.3. , from which the eikonal [9,19]

$$\left[\left(\frac{\partial}{\partial x}\psi(x,y)\right)^2 + \left(\frac{\partial}{\partial y}\psi(x,y)\right)^2\right]^2 = \frac{\rho h(x,y)}{B(x,y)}\omega^2, \tag{22}$$

is obtained from the ϵ^0 order terms, where $\rho h(x,y)$ is the product of the mass density and thickness, and $B(x,y)$ is the plate bending stiffness. Assuming that the material properties vary only along the direction of propagation, i.e. the x axis, then $B(x,y) = B(x)$, and $\rho h(x,y) = \rho h(x)$. Assuming also simply supported edges along $y = 0$, L_y, then the wavenumber components in the y-direction are $k_{ym} = m\pi/L_y$, with $m = 1,2,3\ldots$. It is then possible to derive expressions for the wavenumbers $k_{x1m,x2m}(x)$ and the wave amplitude ratios $A_{xm0}(x)/A_{xm0}(x_0)$ for the mth wave mode [19]. Expressions for the nodal force and DOF vectors $\boldsymbol{\phi}_f^{\pm}$ and $\boldsymbol{\phi}_q^{\pm}$ of the wave modes and the propagation matrices $\boldsymbol{\Lambda}^{\pm}(x_a, x_b)$ are given in Appendix A.3. From these the directly excited waves $\mathbf{e}^{\pm}$ and reflection matrices $\boldsymbol{\Gamma}_{R,L}$ can be calculated.

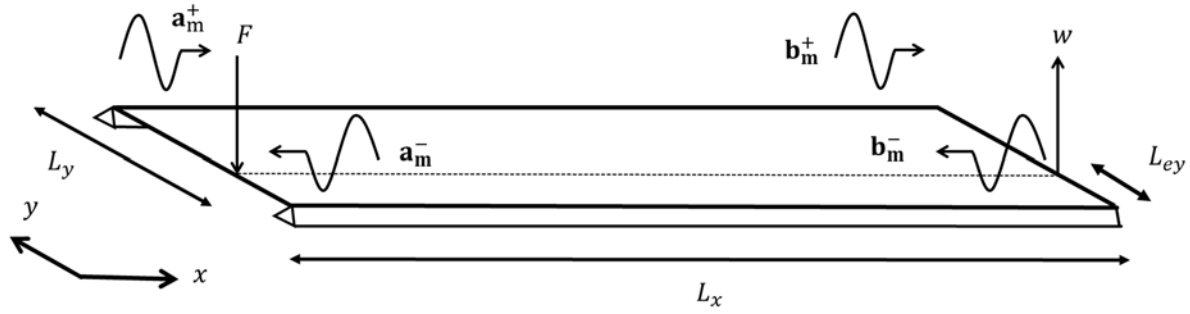

Figure 13. Finite length plate strip with slowly varying material properties undergoing flexural vibrations.

In the following sections, two sets of results are presented. The first considers a linear variation of the plate thickness along its length while the second considers variability of the Young's modulus along the plate strip in the same way as previous examples. Both examples use a steel plate strip with uniform mass density $\rho = 7800$ kg/m^3 and nominal Young's modulus $E_0 = 210$ GPa, with total length $L_x = 5$ m, width $L_y = 1.2$ m. Point excitation is applied at the left boundary with $L_{ey} = 0.21$ m and the response calculated at the right boundary in steps of 0.5 Hz. In this case, the number of WFE evaluations reduces to $N_{eval} = N_{gl} + 2$, further reducing the computational cost. The plate strip has simply supported edges and free-free boundary conditions at the ends. Structural damping is included using a complex Young's modulus $E(1 + \mathrm{i}\eta)$, with $\eta = 10^{-3}$. A total of eight wave modes are used for all of the numerical simulations, among which there are two fundamental wave-types $k_{x1m}(x)$ and $k_{x2m}(x)$, for $m = 1,2,3,4$. This was enough to achieve convergence of the forced response in the frequency band and, in particular, to accurately resolve the antiresonances. The $k_{x1m}(x)$ waves can be evanescent or propagating depending on the frequency and position while the $k_{x2m}(x)$ waves are fundamentally evanescent waves and attenuate more quickly than $k_{x1m}(x)$.

5.3.1. Variable thickness

In this case, the thickness varies from 10 mm to 21 mm, as shown in Figure 14, and $N_{gl} = 3$ integration points are used. Figure 15 presents the transfer receptance obtained from both the analytical solution and from the proposed slowly varying WFE approach, assuming $\eta = 10^{-3}$. Note that, unlike the previous examples, because the excitation and response are not in the middle of the structure, only the phase and amplitude changes between the boundaries need to be calculated. The relative error between the proposed approach and the WKB approximation, Eq. (18), for $N_{gl} = 3$ is shown in Figure16 using 10 equally spaced non-overlapping frequency bands of width $B = 8.2$ Hz and frequency increments of 0.005 Hz, which is 0.1 times the half-power bandwidth at the centre of the frequency range under consideration. No significant improvement is found by increasing N_{gl}. Overall, for $\eta = 10^{-3}$, the error levels are lower than 0.1% but for the last frequency which is lower than 0.15%. Moreover, for $\eta = 10^{-2}$, the error levels are lower than 0.05% at the low frequencies decreasing until the frequency band around 62 Hz, where it increases again to 0.2%.

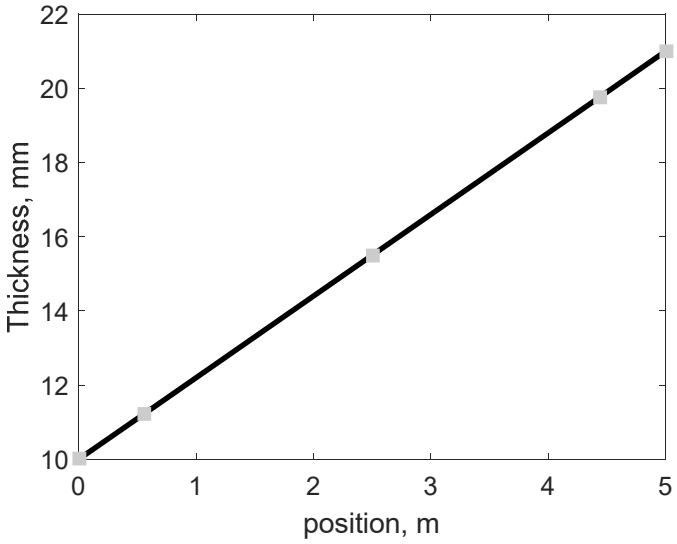

Figure 14. Plate strip thickness as a function of the position along its length and GL quadrature points (grey squares).

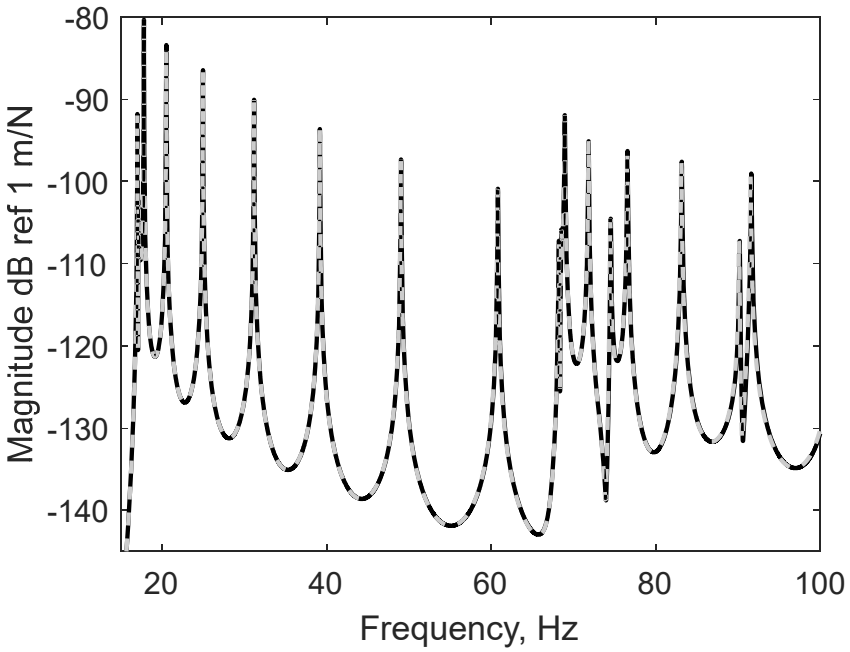

Figure 15. Plate strip with linearly varying thickness: magnitude of the transfer receptance from the left to the right ends obtained from the WKB method (black) and from the WFE approach (dashed grey).

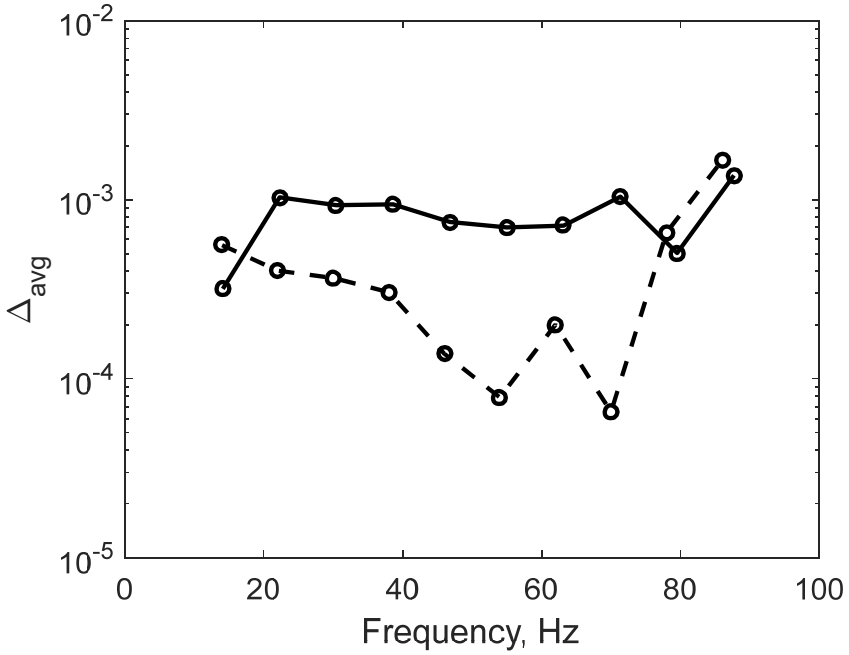

Figure 16. Plate strip with linearly varying thickness: relative error of the frequency averaged magnitude of the transfer receptance from the left to the right ends for $N_{gl} = 3$ with $\eta = 10^{-3}$ (full line) and $\eta = 10^{-2}$ (dashed line), compared to the WKB method.

5.3.2. Variable Young's modulus

Figure 17 shows the phase change and attenuation constant for a plate strip with the varying Young's modulus shown in Figure 18 and neglecting damping. Positive values indicate the real parts of the wavenumbers and negative values indicate imaginary parts. Note that because the wavenumber in the WKB approximation is a function of position, i.e. $k_{1,2m}(\omega) = k_{1,2m}(\omega, x)$, it is possible that, at some frequency ω, a particular wave mode might be a propagating wave, i.e. real wavenumber, and a non-propagating wave, i.e. imaginary wavenumber, at different positions along the plate strip, giving rise to a critical section. They can be recognised in the frequency bands where $\theta(0, L_x)$ has both real and imaginary parts. These turning points cause internal reflection in the plate strip, due to the sudden change of wavenumber characteristics along the plate strip, even though the Young's modulus is slowly varying. These frequency bands generally lie around the cut on frequencies of the wave modes in the homogeneous plate strip, for which the Young's modulus takes its nominal value E_0. It is possible that more than one turning point, or critical section, exist at the same frequency but in different locations along the plate strip. Determining the exact position of these critical sections or the number of occurrences is not within the scope of this paper. Additionally, Figure 19 presents the magnitude of the transfer receptance obtained from the proposed approach, the analytical WKB approximation and the full FE model, assuming $\eta = 10^{-3}$. The slowly varying WFE method is equivalent to the WKB approximation only to the leading order, and the approximation of the wave amplitude change, Eq. (A.17), in Appendix A.3. , might suffer from numerical differences at the critical sections, which might explain the differences from the proposed approach to the WKB approximation at these frequencies. Responses in these frequency bands have to be treated separately and will be subject of future work. The relative error between the proposed approach and the FE model, Eq. (18), is shown in Figure 20 for $N_{gl} = 6$ and $N_{gl} = 8$ with $\eta = 10^{-3}$ and for $N_{gl} = 9$ with $\eta = 10^{-3}$, using 10 equally spaced non-overlapping frequency bands of width $B = 7.7$ Hz and frequency increments of 0.005 Hz, equivalent to 0.1 times the half-power bandwidth at the centre of the frequency range under. It is observed that for

$\eta = 10^{-2}$, the errors are smaller than 2% close to the first turning point and then decrease until the second turning point is reached. At the latter point the errors increase, but are still less than 4% before decreasing again as the frequency is further increased. For $\eta = 10^{-3}$, the error levels are of 14% in the first turning point frequency band, decreasing to less than 4% until the second turning point frequency band, where it increases again to 8%. Despite the large errors at the turning point frequencies, differences at the resonance frequencies are not larger than 0.2% for $\eta = 10^{-3}$ and much smaller for $\eta = 10^{-2}$.

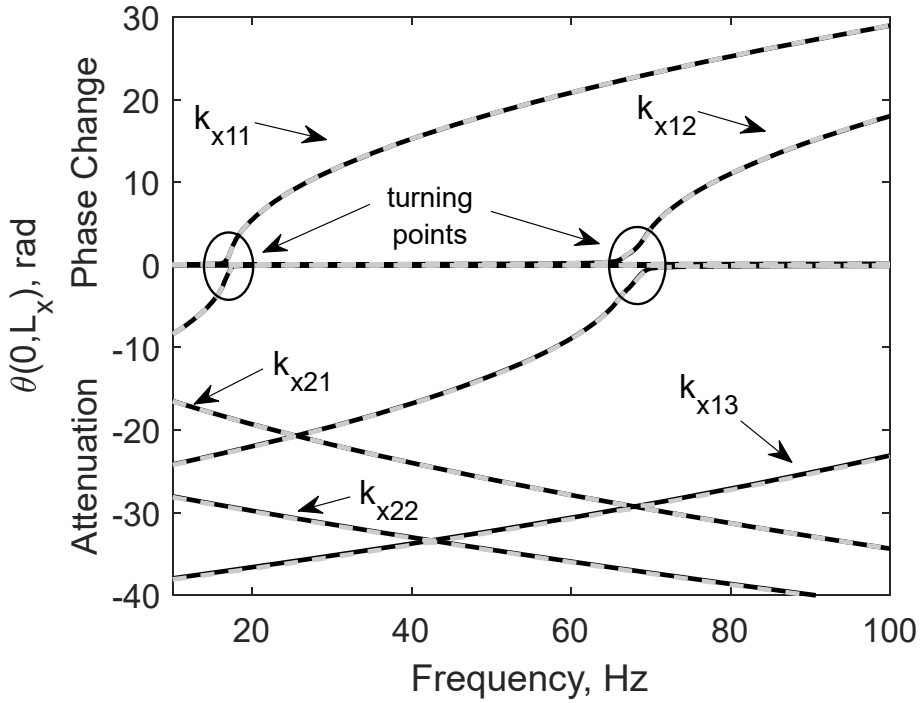

Figure 17. Phase change (positive values) and attenuation constant (negative values) over the plate length for $k_{\mathrm{x}1m}(\omega, x)$ and $k_{\mathrm{x}2m}(\omega, x)$ from the analytical model (black) and from the WFE approach (dashed grey). Positive values are the real part (propagating waves) and negative values are the imaginary part (non-propagating waves). Frequency bands with turning points are highlighted.

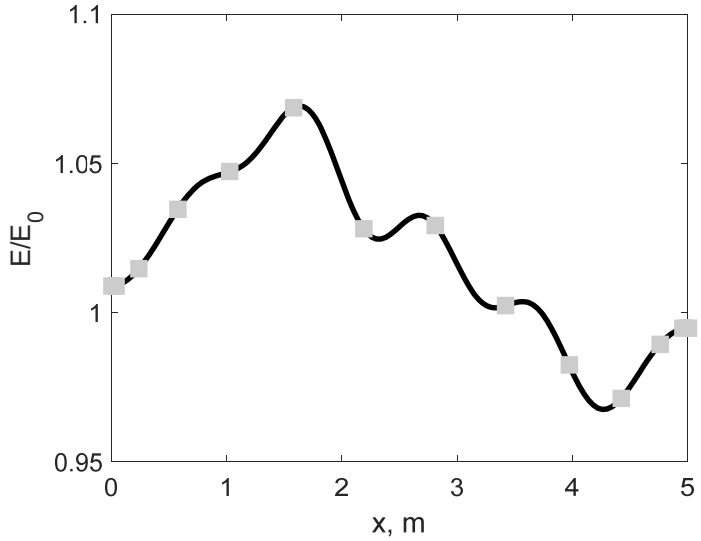

Figure 18. The normalized Young's modulus as a function of the position used for the plate strip. Also shown are the WFE evaluation points (square symbols).

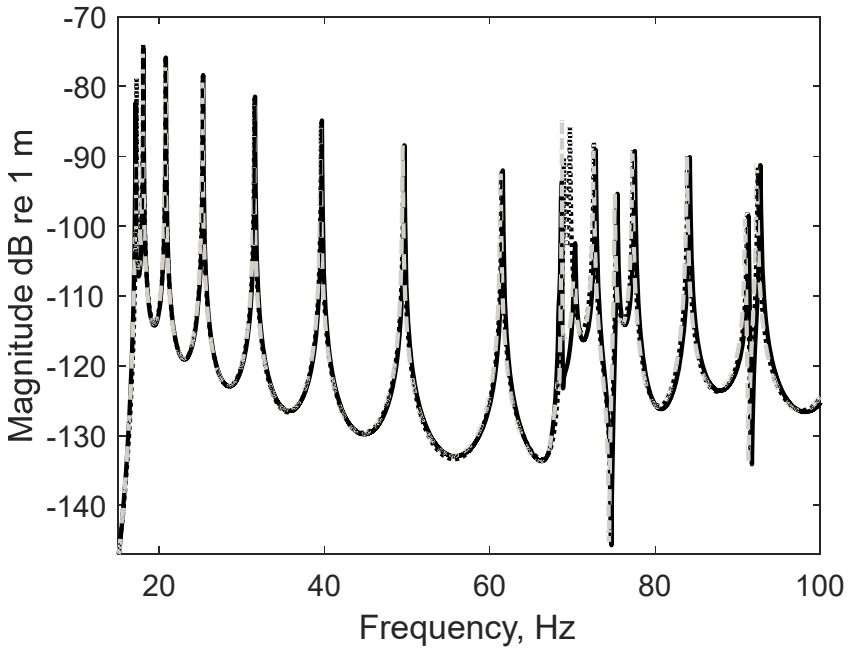

Figure 19. Plate strip: magnitude of the transfer receptance from the left to the right ends obtained from the WKB method (full line), from the slowly varying WFE approach (dashed grey) and from the FE model (dotted line) with varying Young's modulus.

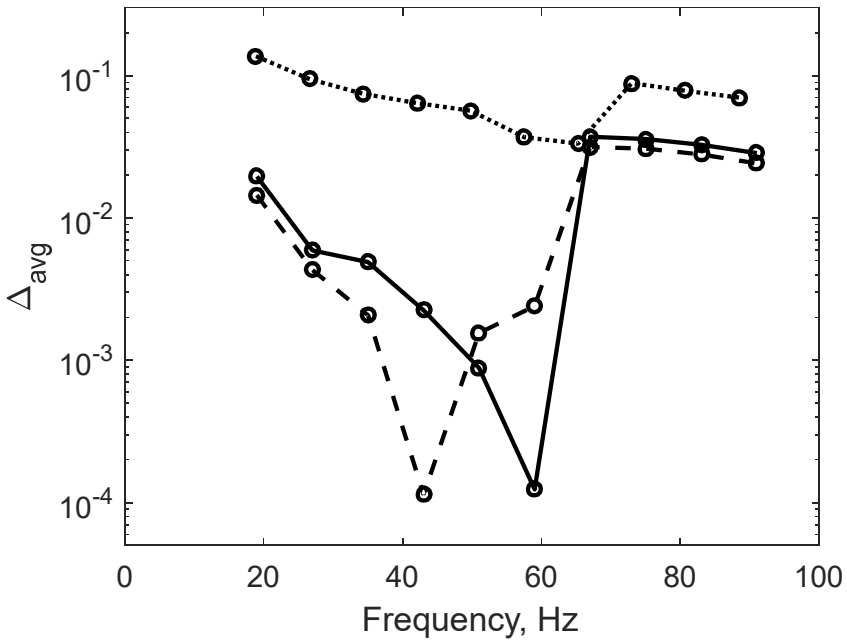

Figure 20. Plate strip with varying Young's modulus: relative error of the frequency averaged magnitude of the transfer receptance, compared to a full FE model, with $N_{gl} = 8$ and $\eta = 10^{-3}$ (dotted line) and with $N_{gl} = 6$ (solid line) and $N_{gl} = 8$ (dashed line) for $\eta = 10^{-2}$.

6. Random variability of waveguide properties

Spatially distributed randomness can be modelled by the well-established random field theory using a probability measure. There are a number of methods available in the literature for generating random fields [16,17,38,39], including formulations using series expansions that are able to represent the field using deterministic spatial functions and random uncorrelated variables. The KL expansion is a special case where these deterministic spatial functions are orthogonal and derived from the correlation function.

A homogeneous random field $H(x)$ with a finite, symmetric and positive definite correlation function $C_H(x_1, x_2)$, defined over a domain D, has a spectral decomposition in the generalized series [17]

$$H(x) = H_0(x) + \sum_{j=1}^{\infty} \sqrt{l_j}\, \xi_j f_j(x), \tag{23}$$

where ξ_j are random variables and l_j and $f_j(x)$ are eigenvalues and eigenfunctions of $C_H(x_1, x_2)$. The eigenvalues and eigenfunctions can be ordered in descending order of eigenvalues and the KL expansion is then truncated at a finite number of terms N_{KL}, chosen by the accuracy of the series in representing the correlation function [41]. As a rule of thumb, N_{KL} can be chosen such that $l_{N_{KL}}/l_1 < 0.1$, and N_{KL} will depend on the correlation length of the random field.

The random variables ξ_j are obtained from the projection of Eq. (23) on its corresponding eigenfunction

$$\xi_j = \frac{1}{\sqrt{l_j}} \int_D H(x)\, f_j(x)\, dx. \tag{24}$$

If $H(x)$ is a Gaussian random field, ξ_j are always Gaussian random variables, therefore this projection does not need to be evaluated. If, on the other hand, the random field is not Gaussian, then the variables ξ_j have unknown joint probability density function (PDF). Therefore, it is not possible to use the KL expansion to directly generate a non-Gaussian random field. However, this issue can be overcome by using another method for simulating a random field and for finding ξ_j. For that end, the Memoryless Non Linear Transformation (MNLT) can be used. This is defined such that $Y(x) = F_Y^{-1}\big(F_H(H(x)\big)$, [42,43] where $F_Y^{-1}(x)$ is the inverse marginal cumulative distribution of the targeted non-Gaussian process and $F_H(x)$ is the standard Gaussian cumulative distribution function (CDF). Despite its simplicity, this has the drawback of altering the correlation function $C_Y(x_1, x_2)$ of the non-Gaussian process from $C_H(x_1, x_2)$ of the underlying Gaussian process. Therefore, the problem can be stated in terms of finding the appropriate $C_H(x_1, x_2)$ for a prescribed $C_Y(x_1, x_2)$, which is not a trivial task. For a limited number of cases, it is possible to find an analytical relation between the two correlation functions [44], otherwise a numerical scheme must be employed [43]. For instance, if the non-Gaussian random field has a Gamma distribution then $C_Y(x_1, x_2) = C_H^2(x_1, x_2)$.

On the other hand, an iterative scheme can be used that maintains the correlation structure of the underlying Gaussian process and adjusts the targeted CDF by applying a MNLT and updating ξ_j until convergence is achieved [45,46]. It has the advantage of directly using the KL expansion and can simulate both stationary and non-stationary random fields as well as strongly non-Gaussian targeted CDF [47]. Moreover, if the target CDF is approximately Gaussian, only one iteration might be enough to achieve convergence.

For some families of correlation functions and specific geometries, there exist analytical solutions. One such case is the one dimensional exponentially decaying autocorrelation function, $C_H(x_1, x_2) = \mathrm{e}^{-|x_1 - x_2|/l_c}$, where l_c is the correlation length, in the interval $-L/2 \leq x \leq L/2$, where L is the length of the domain and where x_1 and x_2 are any two points within the interval. In this case, the KL expansion, for a zero-mean random field, can be written as [17]

$$H(x) = \sum_{j=1}^{N_{kl}} \big[\alpha_j \xi_{1j} \sin\big(w_{1j} x\big) + \beta_j \xi_{2j} \cos\big(w_{2j} x\big)\big] \tag{25}$$

where ξ_{1j} and ξ_{2j} are zero-mean, unity standard deviation, independent random variables and $\alpha_j = \sqrt{l_{1j}/\left(\frac{L}{2} - \frac{\sin(w_{1j}L)}{2w_{1j}}\right)}$, $\beta_j = \sqrt{l_{2j}/\left(\frac{L}{2} + \frac{\sin(w_{2j}L)}{2\mathrm{w}_{2\mathrm{j}}}\right)}$, in which $l_{1\mathrm{j}} = 2c/\big(w_{1i}^2 + c^2\big)$, $l_{2j} = 2c/\big(w_{2i}^2 + c^2\big)$, $c = 1/l_c$ and w_{1i} and $\mathrm{w}_{2\mathrm{i}}$ are the i^{th} roots of the transcendental equations $c \tan w_1 + w_1 = 0$ and $w_2 \tan w_2 - c = 0$, respectively. Note that the trigonometric terms of this equation are the eigenfunctions and the α_j and β_j parameters are given by the eigenvalues divided by the normalization constants of the eigenfunctions. This expansion is truncated to N_{KL} terms according to the magnitudes of the higher order eigenvalues in the series. A complete derivation can be found in the book by Ghanem and Spanos [17].

In the numerical examples, the Young's modulus is chosen to be randomly varying as $E(x) = E_0\big(1 + H(x)\big)$, where E_0 is the nominal value and $H(x)$ is a random field with Gamma marginal PDF given by

$$f_H(x) = \frac{x^{a_0-1}\exp\left(-\frac{x}{b_0}\right)}{b_0^{a_0}\,\Gamma(a_0)}), \qquad \text{for } x > 0, \tag{26}$$

where $\Gamma(x) = \int_0^\infty t^{x-1}e^{-t}\mathrm{d}t\,, x > 0$ is the Gamma function and the parameters of the distribution are given by $a_0 = 1/\delta_E^2$ and $b_0 = E_0\delta_E^2$, where δ_E is the dispersion parameter. This choice of distribution follows the Maximum Entropy argument, and ensures the second-order statistics of the response are finite [15].

Finally, the Latin Hypercube sampling (LHS) scheme [48,49] is used as the stochastic solver. The LHS has the advantage of being as general as the classical Monte Carlo solver, in which given the probability measure of the random variables several samples are generated and the statistics of the response can be evaluated, but with increased computational efficiency, by reducing the required number of realizations.

6.1. Numerical results

In this section, the previous numerical examples of rod, beam and plate strip with spatially varying Young's modulus are now revisited and considered to have random variability, i.e. variability across the ensemble due to random variations in properties at a specific location. This is typically the case when manufacturing variability is taken into account. Material and geometric properties as well as frequency range and steps, number of GL points, FE and WFE discretization parameters are the same as the examples presented in subsections 5.1. to 5.3. Some statistics of the forced response are compared, calculated using the proposed slowly varying WFE approach and the full FE method, with the focus on comparing computational efficiency. Calculations were performed using a MATLAB based implementation and run on a laptop with an Intel CORE i7 processor with 6 GB of RAM.

6.1.1. Thin rod

The random field of the Young`s modulus was generated from the KL expansion assuming $\sigma = 0.1$, correlation length $l_c = 0.5L$ and $N_{kl} = 10$ terms in the KL expansion, enough to represent the field with the required accuracy. One sample of this random field is shown in Figure 4, along with the excitation point and the points used for integration using GL quadrature. The LHS scheme was used as a stochastic solver using 1,000 samples, enough to achieve statistical convergence. Figure 21 presents the 5th and 95th percentiles and the mean value of the input mobility for the stochastic rod using the slowly varying WFE and the standard FE approach and also the input mobility for the homogenous case, i.e. constant Young's modulus E_0 along the rod, for $\eta = 10^{-3}$. In this case, the LHS scheme using the proposed approach was 51 times faster than the standard FE approach.

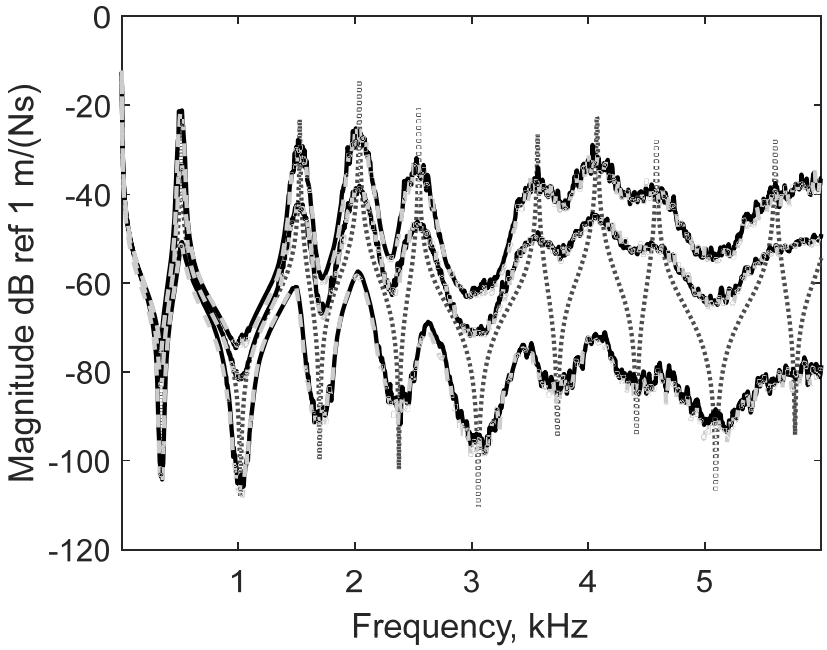

Figure 21. Input mobility of the rod at $x = 0.25L$: magnitude of 5th and 95th percentiles and the mean value using FE (black line) and numerical WKB (grey line) with $\sigma = 0.1$ and $l_c = 0.5L$. In addition, the input mobility for the homogenous rod (grey dotted line) is shown.

6.1.2. Thin beam

Similar to the previous case, the statistics of the input mobility for the stochastic analysis were calculated with 1000 LHS samples, enough to achieve statistical convergence. The Young's modulus random field was also generated using $N_{kl} = 10$ terms with $\sigma = 0.1$ and correlation length $l_c = 0.5L$ in the KL expansion, which is fifty times larger than the length Δ of the segments used for each WFE analysis, and 15 times larger than the element size for the standard FE approach. Figure 22 shows magnitude of the mean and 5th and 95th percentiles of the input mobility calculated using a standard FE approach, the slowly varying WFE and the analytical WKB approximation, for $\eta = 10^{-3}$. The LHS scheme using the proposed approach was 5.5 times faster than the standard FE approach.

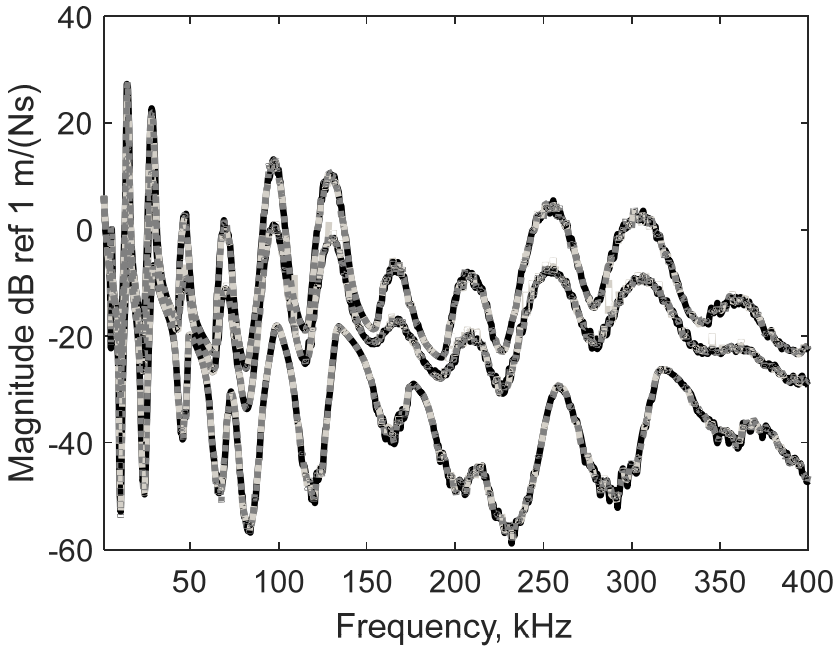

Figure 22. Input mobility of the beam at $x = 0.25L$: magnitude of the mean and 5th and 95th percentiles of the using FE (black solid), slowly varying WFE (dark grey dotted) and numerical WKB (light grey dashed) using $\sigma = 0.1$ and $l_c = 0.5L$.

6.1.3. Plate strip

The aluminium plate strip with simply supported edges is considered to have the Young's modulus as a random field varying only in the direction of the propagating wave, i.e. the x-axis. Effectively, a one-dimensional random field can be used, similar to the rod and beam cases. The statistics of the transfer receptance with $\eta = 10^{-2}$ for the stochastic analysis are calculated from a LHS scheme with 500 samples. which was enough to achieve statistical convergence. Figure 23 shows the mean, 5th, and 95th percentiles of the transfer mobility obtained from the LHS simulation calculated using the WKB approach and the proposed slowly varying WFE approach. The proposed approach was 1.6 times faster than the standard FE approach to calculate the response samples.

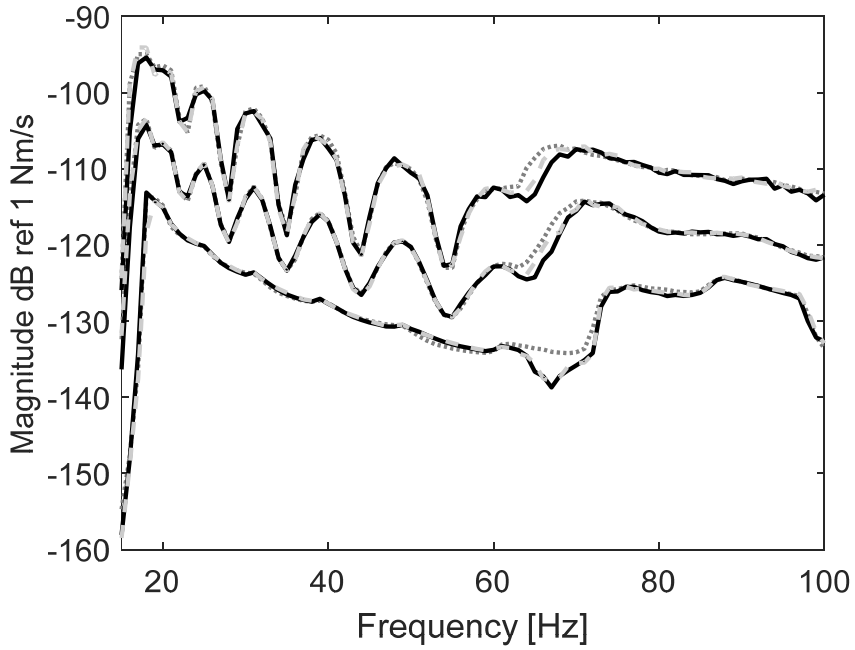

Figure 23. Transfer mobility of the plate strip: magnitude of the mean and 5th and 95th percentiles obtained from the analytical model (black), the WFE approach (dashed grey) and the standard FE (dotted grey).

7. Concluding remarks

A method was proposed to extend the applicability of the WKB approach to cases where no analytical solution to the equations of motion exists by using a Finite Element (FE) approach. The phase change and the attenuation constant require the numerical evaluation of the locally defined wavenumber at various points, which are kept to a minimum, being evaluated at locations defined by a Gauss-Legendre (GL) quadrature scheme. In addition, the WKB solution implies conservation of power (in the undamped case) which is used to calculate the amplitude change.

Examples of typical structural elements with one dimensional wave propagation were used to show the applicability of the proposed approach. These involved longitudinal and flexural waves, with 1 propagating (rod), 2 propagating and nearfield (beam) and multiple (plate strip) wave modes. Results were presented for a deterministic system with varying thickness and Young's modulus, as well as a stochastic analysis, using the Karhunen-Loève (KL) expansion to represent the Young's modulus as a non-Gaussian random field. Even though an analytical KL expansion is used, the method can be extended straightforwardly to a numerical solution of the KL expansion and therefore to different correlation functions or probability density functions. Results in terms of the forced response of finite length waveguides were seen to agree very well with available analytical solutions, the classical analytical WKB approach and full FE analysis. Only a small number of GL points are necessary to calculate the phase and amplitude change, which is required to keep the computational cost to a minimum.

Further steps include extending the proposed approach to more complex waveguides, with different wave modes, exploring other random field types and tackling the turning point problem.

Acknowledgements

The authors gratefully acknowledge the financial support of the Brazilian National Council of Research (CNPq) Process number 445773/2014-6, the Federal District Research Foundation (FAPDF) Process number 0193001040/2015 and the Royal Society for the Newton International Exchanges Fund.

A. Appendix

In this Appendix, some of the results involving analytical expressions for the numerical examples are presented in more detail.

A.1. Longitudinal vibration of thin rods

For a slowly varying thin rod undergoing longitudinal vibration, a FE model for a segment of the rod is built using a single element with two nodes and one degree of freedom per node, with mass and stiffness matrices respectively given by [40]

$$\mathbf{M}_e = \frac{\rho A \Delta}{6}\begin{bmatrix} 2 & 1 \\ 1 & 2 \end{bmatrix} \text{ and } \mathbf{K}_e = \frac{EA}{\Delta}\begin{bmatrix} 1 & -1 \\ -1 & 1 \end{bmatrix}, \tag{A.1}$$

assuming constant properties within each element. Normalizing the displacement by Δ and the force by EA, it is possible to find the transfer matrix as [50]

$$\mathbf{T}(x) = \frac{1}{1+\frac{(k_L(x)\Delta)^2}{6}}\begin{bmatrix} 1-\frac{(k_L(x)\Delta)^2}{3} & -1 \\ (k_L(x)\Delta)^2 - \frac{(k_L(x)\Delta)^4}{12} & 1-\frac{(k_L(x)\Delta)^2}{3} \end{bmatrix}, \tag{A.2}$$

where $k_L(x) = \sqrt{\rho(x)\omega^2/E(x)}$. The transfer matrix eigenvalues are given by

$$\lambda^{\pm}(x) = \frac{1}{1+\frac{(k_L(x)\Delta)^2}{6}}\left[1-\frac{(k_L(x)\Delta)^2}{3} \pm \mathrm{i}k_L\Delta\sqrt{1-\frac{(k_L(x)\Delta)^2}{12}}\right], \tag{A.3}$$

For small values of $k_L(x)\Delta$, they are approximately equal to $\exp(\pm\,\mathrm{i}k_L(x)\Delta)$ and the FE discretization gives accurate values for $k_L(x)\Delta \ll \sqrt{12}$. The WFE wavenumber is given by $k_L(x) = (\mathrm{i}/\Delta)\log\lambda(x)$, which is used to calculate the phase change by evaluating the wavenumber at the positions defined by the GL quadrature scheme, Eq. (14). The amplitude change is calculated from Eq. (16) with

$$\left|\frac{b^+}{a^+}\right| = \sqrt{\frac{k_L(x_a)}{k_L(x_b)}}\sqrt[4]{\frac{1-[k_L(x_a)\Delta]^2/12}{1-[k_L(x_b)\Delta]^2/12}}, \tag{A.4}$$

and using the wave modes [50]

$$\phi_q^+(x) = -\frac{1}{\sqrt{2}\mathrm{i}k_L(x)\Delta\sqrt{1-\frac{[k_L(x)\Delta]^2}{12}}} \quad \text{and} \quad \phi_f^+(x) = \frac{1}{\sqrt{2}}. \tag{A.5}$$

Under the same assumption, i.e. for $k_L\Delta \ll \sqrt{12}$, Eq. (A.4) is approximately equal to the exact solution obtained from the WKB approach [18], i.e. $|b^+|/|a^+| \approx \sqrt{k_L(x_a)/k_L(x_b)}$.

A.2. Flexural vibration of thin beams

This section summarizes an analytical solution for the governing equation of a thin beam undergoing flexural vibration and assuming that the material properties of the beam are constant while the cross-sectional area and the second moment of area are given by $A(x) = \alpha_A x^\mu$ and $I(x) = \alpha_I x^{\mu+2}$, where $\alpha_A > 0$, $\alpha_I > 0$, $x > 0$ and $\mu \geq 0$ is the flaring index. Note that there is a fictitious vertex at $x = 0$ and the position $x = x_L$ and $x = x_R$ at the left and right sides of the beam are defined by the choice of both h_L and h_R, i.e. the thickness at both sides of the beam, as well as the beam length L. An analytical solution of Eq. (19) can be found in terms of a linear combination of Hankel and modified Bessel functions representing positive and negative going propagating and evanescent waves, such that [4]

$$\begin{aligned} W(x) = x^{-\mu/2}\Big[&C_1 H_\mu^{(2)}(2k_B(x)x) + C_2 K_\mu(2k_B(x)x) + C_3 H_\mu^{(1)}(2k_B(x)x) \\ &+ C_4 I_\mu(2k_B(x)x)\Big], \end{aligned} \tag{A.6}$$

where C_1, C_2, C_3, C_4 are arbitrary constants, $H_\mu^{(1,2)}(2k_B(x)x)$ is the Hankel function of the first and second kind, of order μ and argument $2k_B(x)x$ and $I_\mu(2k_B(x)x)$ and $K_\mu(2k_B(x)x)$ are the modified Bessel functions of the first and second kind of order μ Expressions for the displacement and internal forces matrices for positive and negative going waves are given by

$$\boldsymbol{\Phi}_q^+ = \begin{bmatrix} 1 & 1 \\ -k_B(x)\dfrac{H_{\mu+1}^{(2)}(2k_B(x)x)}{H_\mu^{(2)}(2k_B(x)x)} & k_B(x)\dfrac{K_{\mu+1}(2k_B(x)x)}{K_\mu(2k_B(x)x)} \end{bmatrix}, \tag{A.7}$$

$$\boldsymbol{\Phi}_q^- = \begin{bmatrix} 1 & 1 \\ -k_B(x)\dfrac{H_{\mu+1}^{(1)}(2k_B(x)x)}{H_\mu^{(1)}(2k_B(x)x)} & k_B(x)\dfrac{I_{\mu+1}(2k_B(x)x)}{I_\mu(2k_B(x)x)} \end{bmatrix}, \tag{A.8}$$

$$\boldsymbol{\Phi}_f^+ = EI(x)\begin{bmatrix} -k_B^3(x)\dfrac{H_{\mu+1}^{(2)}(2k_B(x)x)}{H_\mu^{(2)}(2k_B(x)x)} & k_B^3(x)\dfrac{K_{\mu+1}(2k_B(x)x)}{K_\mu(2k_B(x)x)} \\ k_B^2(x)\dfrac{H_{\mu+2}^{(2)}(2k_B(x)x)}{H_\mu^{(2)}(2k_B(x)x)} & k_B^2(x)\dfrac{K_{\mu+2}(2k_B(x)x)}{K_\mu(2k_B(x)x)} \end{bmatrix}, \tag{A.9}$$

$$\boldsymbol{\phi}_f^- = EI(x)\begin{bmatrix} -k_B^3(x)\dfrac{H_{\mu+1}^{(1)}(2k_B(x)x)}{H_\mu^{(1)}(2k_B(x)x)} & -k_B^3(x)\dfrac{I_{\mu+1}(2k_B(x)x)}{I_\mu(2k_B(x)x)} \\ k_B^2(x)\dfrac{H_{\mu+2}^{(1)}(2k_B(x)x)}{H_\mu^{(1)}(2k_B(x)x)} & k_B^2(x)\dfrac{I_{\mu+2}(2k_B(x)x)}{I_\mu(2k_B(x)x)} \end{bmatrix}, \tag{A.10}$$

i.e., $\boldsymbol{\phi}_q^+$, $\boldsymbol{\phi}_q^-$, $\boldsymbol{\phi}_f^+$ and $\boldsymbol{\phi}_f^-$ can be found analytically in terms of these functions. The positive and negative going propagation matrices between x_a and x_b can be defined as [4]

$$\boldsymbol{\Lambda}^+(x_a, x_b) = \mathrm{diag}\left\{\left(\frac{x_a}{x_b}\right)^{\mu/2}\frac{H_\mu^{(2)}\left[2k_B(x_a)(x_a x_b)^{1/2}\right]}{H_\mu^{(2)}\left(2k_B(x_a)\right)}, \frac{K_\mu\left[2k_B(x_a)(x_a x_b)^{1/2}\right]}{K_\mu(2k_B(x_a)x_a)}\right\}, \tag{A.11}$$

$$\boldsymbol{\Lambda}^-(x_b, x_a) = \mathrm{diag}\left\{\left(\frac{x_b}{x_a}\right)^{\mu/2}\frac{H_\mu^{(1)}(2k_B(x_a)x_a)}{H_\mu^{(1)}[2k_B(x_a)(x_a x_b)^{1/2}]}, \frac{I_\mu(2k_B(x_a)x_a)}{I_\mu[2k_B(x_a)(x_a x_b)^{1/2}]}\right\}. \tag{A.12}$$

The amplitudes of the positive and negative going waves generated by a point excitation at $x = L_e$ are identical and are given by [4]

$$\mathbf{e}^\pm = -\frac{f_{ext}L_e}{4EI(L_e)k_B^2(L_e)}\begin{Bmatrix} \mathrm{i}\pi\left|H_\mu^{(2)}(2k_B(x_a)x_a)\right| \\ 4K_\mu(2k_B(x_a)x_a)I_\mu(2k_B(x_a)x_a) \end{Bmatrix}, \tag{A.13}$$

Moreover, reflection matrices can be found by using Eq. (11), and the forced response can be calculated from Eqs. (5) and (6). More details on this formulation can be found in [4].

A.3. Flexural vibration in a thin plate strip

This section presents the analytical solution of the WKB approach for a plate strip of constant width with simply supported edges and slowly varying properties along the length of the plate strip, summarized from [19]. Considering a thin plate undergoing out-of-plane flexural vibration with varying material properties, assuming solutions of the kind $w(x,y) = A(x,y)\mathrm{e}^{-\mathrm{i}\frac{\psi(x,y)}{\epsilon}}$, where $w(x,y)$ is the out-of-plane displacement and the amplitude is expanded in terms of the parameter ϵ as $A(x,y) = A_0(x,y) + A_1(x,y)\epsilon$ it is possible to match the terms with equal powers of ϵ on both left and right hand side of the governing equation

This procedure leads to a number of differential equations, which need to be solved for each term in the expansion. From $\psi(x,y)$, one can find the eikonal equation for the phase change in Eq. (22) and the terms of ϵ give expressions for the amplitude terms. However, if a plate strip with simply supported boundary conditions at $y = 0$ and $y = L_y$ is considered, also assuming material variability only in the direction of propagation, i.e. the x axis, then $B(x,y) = B(x)$, and $\rho h(x,y) = \rho h(x)$, where $\rho h(x,y)$ is the product of the mass density and thickness, and $B(x,y)$ is the plate bending stiffness and it is possible to assume phase change of the form $\psi_m(x,y)/\epsilon = \theta_{xm}(x) + k_{ym}y$, where $k_{ym} = m\pi/L_y$ is the m^{th} wave mode in the y direction and $\theta_{xm}(x)$ is the phase change in the x direction. This expression can be used for direct integration of the eikonal equation leading to

$$\theta_{xm}(x_0, x) = \int_{x_0}^{x} k_{xm}(\xi)\, d\xi, \tag{A.14}$$

with four solutions for the phase change in the x direction, where $k_{x1m,x2m}(x) = \pm\sqrt{\pm k_p^2(x) - k_{ym}^2}$, $k_p(x) = \sqrt{\omega}\left(\frac{\rho h(x)}{B(x)}\right)^{1/4}$ is the local free bending wavenumber in the thin plate and x_0 is an arbitrary point in the waveguide. From this it is possible to distinguish two wave types, $k_{x1m}(x)$ and $k_{x2m}(x)$. For a plate strip with simply supported edges, the displacement can be written as

$$w(x, y) = \sum_{m=1}^{\infty} w_m(x) \sin(k_{my} y), \tag{A.15}$$

and therefore for the m^{th} wave mode, the amplitude change can be written using only the first order as $A_m(x, y) = [A_{xm0}(x) + A_{xm1}(x)\epsilon] \sin(k_{my} y)$. The amplitude term $A_{xm0}(x, y)$ is found from matching the ϵ^0 order of the expansion and using the solution for the phase term $\psi_m(x, y)$ and for $k_p^2(x) \gg 0$. From this it is possible to obtain the differential equation,

$$\frac{2}{A_{xm0}} \frac{\partial A_{xm0}}{\partial x} + \frac{1}{\theta_{xm}(x)} \frac{\partial \theta_{xm}(x)}{\partial x} = 0, \tag{A.16}$$

whose solution gives the typical WKB expression for the change in wave amplitude

$$A_{xm0}(x) = \frac{A_{xm0}(x_0)\sqrt{k_{xm}(x_0)}}{\sqrt{k_{xm}(x)}}. \tag{A.17}$$

The transformations from the wave domain to the physical domain are given by

$$\mathbf{q} = \begin{bmatrix} w \\ dw/dx \end{bmatrix} = \sum_{\boldsymbol{m}} \boldsymbol{\Phi}_{qm}^{+} \mathbf{a}_{\boldsymbol{m}}^{+} + \boldsymbol{\Phi}_{qm}^{-} \mathbf{a}_{\boldsymbol{m}}^{-} \text{ and } \mathbf{f} = \begin{bmatrix} Q \\ M \end{bmatrix} = \sum_{\boldsymbol{m}} \boldsymbol{\Phi}_{\boldsymbol{fm}}^{+} \mathbf{a}^{+} + \boldsymbol{\Phi}_{fm}^{-} \mathbf{a}^{-}, \tag{A.18}$$

where w is the out-of-plane displacement, Q is the net force and M is the bending moment [51]. The propagation matrix for the m_{th} mode is given by

$$\begin{aligned} \boldsymbol{\Lambda}_{\boldsymbol{m}}^{+}(x_a, x_b) &= \mathrm{diag}\left[\exp\left(-\mathrm{i}\phi_{xm}(x_a, x_b) + \gamma_m(x_a, x_b)\right)\right], \\ \boldsymbol{\Lambda}_{\boldsymbol{m}}^{-}(x_b, x_a) &= \mathrm{diag}\left[\exp\left(-\mathrm{i}\phi_{xm}(x_a, x_b) - \gamma_m(x_a, x_b)\right)\right], \end{aligned} \tag{A.19}$$

where $\gamma_m(x_a, x_b)$ is obtained from Eq. A.17. Moreover, the displacement and force wave mode matrices are given by

$$\boldsymbol{\Phi}_{\mathrm{qm}}^{+} = \sin(k_{my} y) \begin{bmatrix} 1 & 1 \\ -\mathrm{i}k_{x1m} & -\mathrm{i}k_{x2m} \end{bmatrix}, \boldsymbol{\Phi}_{\mathrm{qm}}^{-} = \sin(k_{my} y) \begin{bmatrix} 1 & 1 \\ \mathrm{i}k_{x1m} & \mathrm{i}k_{x2m} \end{bmatrix},$$

$$\boldsymbol{\Phi}_{\mathrm{fm}}^{+} = \sin\left(k_{my} y\right) B(x) \begin{bmatrix} k_{x1m}^2 + \nu k_{my}^2 & k_{x2m}^2 + \nu k_{my}^2 \\ -\mathrm{i}k_{x1m}\left(k_{x1m}^2 + (2-\nu)k_{my}^2\right) & -\mathrm{i}k_{x2m}\left(k_{x2m}^2 + (2-\nu)k_{my}^2\right) \end{bmatrix}, \tag{A.20}$$

$$\boldsymbol{\Phi}_{\mathrm{fm}}^{-} = \sin(k_{my}y)\, B(x) \begin{bmatrix} k_{x1m}^2 + \nu k_{my}^2 & k_{x2m}^2 + \nu k_{my}^2 \\ \mathrm{i}k_{x1m}\left(k_{x1m}^2 + (2-\nu)k_{my}^2\right) & \mathrm{i}k_{x2m}\left(k_{x2m}^2 + (2-\nu)k_{my}^2\right) \end{bmatrix}.$$

Reflection matrices at both boundaries and the amplitudes of the positive and negative going wave generated by a point excitation can be calculated by Eqs. (11) and (12), respectively.

References

[1] Q.S. Li, Exact solutions for free longitudinal vibrations of non-uniform rods, J. Sound Vib. 234 (2000) 1–19. doi:10.1006/jsvi.1999.2856.

[2] M. Eisenberger, Exact longitudinal vibration frequencies of a variable cross-section rod, Appl. Acoust. 34 (1991) 123–130. doi:10.1016/0003-682X(91)90027-C.

[3] S. Guo, S. Yang, Wave motions in non-uniform one-dimensional waveguides, J. Vib. Control. 18 (2012) 92–100. doi:10.1177/1077546311399948.

[4] S.K. Lee, B.R. Mace, M.J. Brennan, Wave propagation, reflection and transmission in non-uniform one-dimensional waveguides, J. Sound Vib. 304 (2007) 31–49. doi:10.1016/j.jsv.2007.01.039.

[5] F.P. Bretherton, Propagation in slowly varying waveguides, Proc. R. Soc. Lond. Ser. Math. Phys. Sci. 302 (1968) 555–576. doi:10.1098/rspa.1968.0035.

[6] G.B. Whitham, Linear and nonlinear waves, John Wiley & Sons, New York, 1974.

[7] E.J. Hinch, Perturbation Methods, First, Cambridge, UK, 1991. doi:10.1017/CBO9781139172189.

[8] R.B. Nielsen, N. Peake, Tunnelling effects for acoustic waves in slowly varying axisymmetric flow ducts, J. Sound Vib. 380 (2016) 180–191. doi:10.1016/j.jsv.2016.06.003.

[9] A.D. Pierce, Physical interpretation of the WKB or eikonal approximation for waves and vibrations in inhomogeneous beams and plates, J. Acoust. Soc. Am. 48 (1970) 275–284. doi:10.1121/1.1912125.

[10] R. Nielsen, S. Sorokin, The WKB approximation for analysis of wave propagation in curved rods of slowly varying diameter, Proc R Soc A. 470 (2014) 20130718. doi:10.1098/rspa.2013.0718.

[11] S. Foucaud, G. Michon, Y. Gourinat, A. Pelat, F. Gautier, Artificial cochlea and acoustic black hole travelling waves observation: Model and experimental results, J. Sound Vib. 333 (2014) 3428–3439. doi:10.1016/j.jsv.2014.03.016.

[12] S.W. Rienstra, Sound propagation in slowly varying lined flow ducts of arbitrary cross-section, J. Fluid Mech. 495 (2003) 157–173. doi:10.1017/S0022112003006050.

[13] N.C. Ovenden, A uniformly valid multiple scales solution for cut-on cut-off transition of sound in flow ducts, J. Sound Vib. 286 (2005) 403–416. doi:10.1016/j.jsv.2004.12.009.

[14] N.R.T. Biggs, Wave trapping in a two-dimensional sound-soft or sound-hard acoustic waveguide of slowly-varying width, Wave Motion. 49 (2012) 24–33. doi:10.1016/j.wavemoti.2011.06.004.

[15] C. Soize, Uncertainty Quantification - An Accelerated Course with Advanced Applications in Computational Engineering, 1st ed., Springer, 2017. http://www.springer.com/br/book/9783319543383.

[16] E. Vanmarcke, Random Field: Analysis and Synthesis, 2nd Revised and Expanded, Word Scientific, Cambridge, MA, 2010.

[17] R. Ghanem, P.D. Spanos, Stochastic Finite Elements: A Spectral Approach, Revised edition, Dover Publications, Minneola, N.Y., 2012.

[18] A.T. Fabro, N.S. Ferguson, T. Jain, R. Halkyard, B.R. Mace, Wave propagation in one-dimensional waveguides with slowly varying random spatially correlated variability, J. Sound Vib. 343 (2015) 20–48. doi:10.1016/j.jsv.2015.01.013.

[19] A.T. Fabro, Propagation in waveguides with slowly changing variability, PhD Thesis, University of Southampton, 2014. http://eprints.soton.ac.uk/363111/.

[20] B.R. Mace, D. Duhamel, M.J. Brennan, L. Hinke, Finite element prediction of wave motion in structural waveguides, J. Acoust. Soc. Am. 117 (2005) 2835–2843. doi:10.1121/1.1887126.

[21] J.-M. Mencik, M.N. Ichchou, Multi-mode propagation and diffusion in structures through finite elements, Eur. J. Mech. - ASolids. 24 (2005) 877–898. doi:10.1016/j.euromechsol.2005.05.004.

[22] M.N. Ichchou, S. Akrout, J.M. Mencik, Guided waves group and energy velocities via finite elements, J. Sound Vib. 305 (2007) 931–944. doi:10.1016/j.jsv.2007.05.007.
[23] E. Manconi, B.R. Mace, Wave characterization of cylindrical and curved panels using a finite element method, J. Acoust. Soc. Am. 125 (2009) 154–163. doi:10.1121/1.3021418.
[24] Y. Waki, B.R. Mace, M.J. Brennan, Numerical issues concerning the wave and finite element method for free and forced vibrations of waveguides, J. Sound Vib. 327 (2009) 92–108. doi:10.1016/j.jsv.2009.06.005.
[25] Y. Waki, B.R. Mace, M.J. Brennan, Free and forced vibrations of a tyre using a wave/finite element approach, J. Sound Vib. 323 (2009) 737–756. doi:10.1016/j.jsv.2009.01.006.
[26] J.M. Renno, B.R. Mace, On the forced response of waveguides using the wave and finite element method, J. Sound Vib. 329 (2010) 5474–5488. doi:10.1016/j.jsv.2010.07.009.
[27] J.M. Renno, B.R. Mace, Calculation of reflection and transmission coefficients of joints using a hybrid finite element/wave and finite element approach, J. Sound Vib. 332 (2013) 2149–2164. doi:10.1016/j.jsv.2012.04.029.
[28] J.-M. Mencik, New advances in the forced response computation of periodic structures using the wave finite element (WFE) method, Comput. Mech. 54 (2014) 789–801. doi:10.1007/s00466-014-1033-1.
[29] M.N. Ichchou, F. Bouchoucha, M.A. Ben Souf, O. Dessombz, M. Haddar, Stochastic wave finite element for random periodic media through first-order perturbation, Comput. Methods Appl. Mech. Eng. 200 (2011) 2805–2813. doi:10.1016/j.cma.2011.05.004.
[30] M.A. Ben Souf, O. Bareille, M.N. Ichchou, F. Bouchoucha, M. Haddar, Waves and energy in random elastic guided media through the stochastic wave finite element method, Phys. Lett. A. 377 (2013) 2255–2264. doi:10.1016/j.physleta.2013.06.039.
[31] S. Ben, O. Bareille, M. Ichchou, M. Haddar, The wave finite element method for uncertain systems with model uncertainty, Proc. Inst. Mech. Eng. Part C J. Mech. Eng. Sci. 230 (2015) 974–985. doi:10.1177/0954406215617197.
[32] J.P. Arenas, M.J. Crocker, A note on a WKB application to a duct of varying cross-section, Appl. Math. Lett. 14 (2001) 667–671. doi:10.1016/s0893-9659(01)80024-0.
[33] R.D. Firouz-Abadi, H. Haddadpour, A.B. Novinzadeh, An asymptotic solution to transverse free vibrations of variable-section beams, J. Sound Vib. 304 (2007) 530–540. doi:10.1016/j.jsv.2007.02.030.
[34] J.O. Morsbøl, S.V. Sorokin, N. Peake, A WKB approximation of elastic waves travelling on a shell of revolution, J. Sound Vib. 375 (2016) 162–186. doi:10.1016/j.jsv.2016.04.001.
[35] A.H. Nayfeh, Perturbation methods, Wiley, New York, 1973.
[36] John Heading, An Introduction to Phase-Integral Methods, Reprinted edition, Dover Publications, New York, USA, 2013.
[37] A. Der Kiureghian, J.-B. Ke, The stochastic finite element method in structural reliability, Probabilist Eng. Mech. 3 (1988) 83–91.
[38] G. Stefanou, The stochastic finite element method: Past, present and future, Comput. Methods Appl. Mech. Eng. 198 (2009) 1031–1051. doi:10.1016/j.cma.2008.11.007.
[39] B. Sudret, A. Der Kiuereghian, Stochastic Finite Element methods and reliability: A state-of-Art report, University of California, Berkeley, 2000.
[40] M. Petyt, Introduction to Finite Element vibration analysis, 2nd ed., Cambridge University Press, New York, USA, 2010.
[41] S.P. Huang, S.T. Quek, K.K. Phoon, Convergence study of the truncated Karhunen–Loeve expansion for simulation of stochastic processes, Int. J. Numer. Methods Eng. 52 (2001) 1029–1043. doi:10.1002/nme.255.
[42] M. Schevenels, G. Lombaert, G. Degrande, Application of the stochastic finite element method for Gaussian and non-Gaussian systems, in: Procedings ISMA2004, Leuven, Belgium, 2004. http://bwk.kuleuven.be/apps/bwm/papers/scheip04a.pdf.
[43] G. V. Weinberg, L. Gunn, Simulation of statistical distributions using the memoryless nonlinear transform, Australia, 2011.
[44] R. Vio, P. Andreani, W. Wamsteker, Numerical Simulation of Non-Gaussian Random Fields with Prescribed Correlation Structure, Publ. Astron. Soc. Pac. 113 (2001) 1009–1020. doi:10.1086/322919.

[45] K.K. Phoon, S.P. Huang, S.T. Quek, Simulation of second-order processes using Karhunen–Loeve expansion, Comput. Struct. 80 (2002) 1049–1060. doi:10.1016/S0045-7949(02)00064-0.
[46] K.K. Phoon, H.W. Huang, S.T. Quek, Simulation of strongly non-Gaussian processes using Karhunen–Loeve expansion, Probabilistic Eng. Mech. 20 (2005) 188–198. doi:10.1016/j.probengmech.2005.05.007.
[47] L.B. Li, K.K. Phoon, S.T. Quek, Comparison between Karhunen–Loève expansion and translation-based simulation of non-Gaussian processes, Comput. Struct. 85 (2007) 264–276. doi:10.1016/j.compstruc.2006.10.010.
[48] A. M. J. Olsson, G. E. Sandberg, Latin Hypercube Sampling for Stochastic Finite Element Analysis, J. Eng. Mech. 128 (2002). doi:10.1061/(ASCE)0733-9399(2002)128:1(121).
[49] R.Y. Rubinstein, D.P. Kroese, Simulation and the Monte Carlo method, Second Edition, John Wiley & Sons, Inc., Hoboken, NJ, USA, 2007.
[50] D. Duhamel, B.R. Mace, M.J. Brennan, Finite Element Analysis of the Vibrations of Waveguides and Periodic Structures, University of Southampton, UK, 2003. ISVR Technical Memorandum 922. http://resource.isvr.soton.ac.uk/staff/pubs/PubPDFs/Pub2022.pdf.
[51] K.F. Graff, Wave motion in elastic solids, Dover, 1991.